Open access • Proceedings Article • DOI:10.2514/6.2019-1811

Preliminary Sizing of a Hybrid-Electric Passenger Aircraft Featuring Over-the-Wing Distributed-Propulsion — Source link

R. de Vries, M.F.M. Hoogreef, Roelof Vos

Institutions: Delft University of Technology

Published on: 07 Jan 2019

Topics: Range (aeronautics), Propulsion, Payload, Engineering design process and Turboprop

Preliminary Sizing of a Hybrid-Electric Passenger Aircraft Featuring Over-the-Wing Distributed-Propulsion

de Vries, Reynard; Hoogreef, Maurice; Vos, Roelof

DOI
10.2514/6.2019-1811

Publication date
2019

Document Version
Final published version

Published in
AIAA Scitech 2019 Forum

AIAA SciTech Forum
7-11 January 2019, San Diego, California
AIAA Scitech 2019 Forum

10.2514/6.2019-1811

Preliminary Sizing of a Hybrid-Electric Passenger Aircraft Featuring Over-the-Wing Distributed-Propulsion

Reynard de Vries*, Maurice F. M. Hoogreef† and Roelof Vos‡
Delft University of Technology, Kluyverweg 1, 2629HS Delft, The Netherlands

This study compares a hybrid-electric aircraft featuring a propulsive empennage and over-the-wing, distributed-propulsion to a conventional regional turboprop. The impact of multiple design parameters, mission requirements, and technology assumptions on maximum take-off mass and payload-range energy efficiency is evaluated, in order to illustrate the sensitivities of the design. A preliminary sizing method that incorporates aero-propulsive interaction effects is used to obtain rapid estimations. Results show that, for the baseline mission, the hybrid-electric variant is 2.5% heavier and consumes 2.5% more energy than the reference aircraft. In this process, several key design guidelines and challenges for distributed-propulsion aircraft are identified. Firstly, when comparing a hybrid-electric configuration to a conventional one, each aircraft must be sized at its optimum cruise altitude for the same payload and range requirements. Secondly, the hypothetical advantages of distributed propulsion described in literature do not easily lead to a benefit at aircraft level, if the aero-propulsive interaction effects and associated dependencies are incorporated in the design process. Thirdly, the power-control parameters affect practically all characteristics of the aircraft, and the optimal control strategy is highly dependent on the aero-propulsive interaction. The results suggest that the proposed configuration can constitute a low-noise alternative for the regional transport market if the performance of the over-the-wing distributed-propulsion system is optimized.

Nomenclature

Latin symbols

A	=	Aspect ratio [-]
c	=	Chord [m]
C_{D0}	=	Zero-lift drag coefficient [-]
C_D	=	Drag coefficient [-]
C_L	=	Lift coefficient [-]
D	=	Drag [N] or diameter [m]
e	=	Oswald factor [-]
E	=	Energy [J]
h	=	Altitude [ft]
k	=	Correction factor [-]
L	=	Lift [N]
m	=	Mass [kg]
M	=	Mach number [-]
N	=	Number of propulsors [-]
P	=	Power [W]
R	=	Range [nmi]
R^2	=	Coefficient of determination [-]
S	=	Wing area [m^2]
T_c	=	Thrust coefficient [-]
T	=	Thrust [N]
v	=	Velocity [m/s]
W	=	Weight [N]
x	=	Axial position [m]

Greek symbols

α	=	Angle of attack [deg]
Δ	=	Change w.r.t. reference or zero-thrust conditions [-]
ΔY	=	Wing span-fraction occupied by propulsors [-]
η	=	Efficiency [-]
ξ	=	Throttle [-]
ρ	=	Density [kg/m^3]
φ	=	Shaft power ratio [-]
Φ	=	Supplied power ratio [-]

Additional subscripts

1	=	Primary powertrain or start of mission segment
2	=	Secondary powertrain or end of mission segment
bat	=	Battery
cr	=	Cruise
EM	=	Electrical machine
f	=	Fuel
GT	=	Gas turbine
L	=	Landing
miss	=	Nominal mission
s	=	Shaft
SL	=	Sea level
p	=	Propulsor
PL	=	Payload
TO	=	Take-off

*PhD Candidate, Faculty of Aerospace Engineering, R.deVries@tudelft.nl, AIAA member.
†Postdoctoral Research Associate, Faculty of Aerospace Engineering, M.F.M.Hoogreef@tudelft.nl, AIAA Member
‡Assistant Professor, Faculty of Aerospace Engineering, R.Vos@tudelft.nl, AIAA Associate Fellow.

Abbreviations

COSAR	=	Cost-specific air range
CSP	=	Combined specific power
DOH	=	Degree of hybridization
DOE	=	Design of experiments
DP	=	Distributed propulsion
ESAR	=	Energy-specific air range
HEP	=	Hybrid-electric propulsion
MTOM	=	Maximum take-off mass
OEI	=	One engine inoperative
OTW	=	Over-the-wing
PE	=	Propulsive empennage
PFEE	=	Payload-fuel energy efficiency
PMAD	=	Power management and distribution
PREE	=	Payload-range energy efficiency
PSEC	=	Productivity-specific energy consumption
PTE	=	Partial turboelectric
SP	=	Specific power
SPPH	=	Series/parallel partial hybrid
TV	=	Thrust vectoring

I. Introduction

The use of hybrid-electric propulsion (HEP) has been analyzed throughout a wide range of studies over the last decade, as a potential candidate to reduce operating costs and the environmental impact of aviation. Advantages of HEP include emission-free missions or flight phases [1–3], optimization of powertrain efficiency through electrically-assisted propulsion [4], and the possibility to efficiently distribute power to different locations on the airframe. This last benefit is commonly referred to as *distributed propulsion* (DP) [5], which enables advanced propulsion-system layouts with increased aero-propulsive efficiency [6, 7], reduced noise emissions through shielding [8], or enhanced high-lift [6, 9] and control [10] capabilities. However, due to the battery weight penalty associated to many hybrid-electric powertrains, most design studies evaluate reduced ranges [2, 3, 11, 12] or require battery technology levels which are inconceivable in the near future [13–15] in order to make these aircraft concepts viable.

It is therefore evident that, in order to achieve ranges comparable to non-HEP commercial transport aircraft ($R \geq 800$ nmi) in the coming decades, large HEP aircraft must feature either few batteries, or no batteries at all. Although these two options may seem similar, the underlying design philosophies are very different. An example of the former is the parallel or "boosted" turbofan, which aims to improve the powertrain's efficiency through improved well-to-shaft energy transmission, or by down-sizing the gas turbine to its on-design operating conditions [16, 17]. In this case, only minor modifications to the airframe are required. The latter, on the other hand, is known as "turboelectric" propulsion, and aims at improving the aerodynamic efficiency of the airframe or the propulsive efficiency of the jets, propellers, or fans (see e.g. Refs. [9, 18]), rather than the well-to-shaft conversion efficiency of the powertrain. These powertrains typically imply radical changes to the external layout of the aircraft. Logically, both strategies can be combined to form more advanced powertrain architectures such as the "series-parallel partial-hybrid" (SPPH) architecture [19]. Although this further increases the number of possible propulsion-system configurations, a systematic evaluation of the design space is generally hindered by the low technology readiness level of hybrid-electric powertrain components and the lack of detailed propulsion-airframe integration studies. Thus, in an effort to further explore the design space, this paper presents a preliminary sizing study of a hybrid-electric aircraft featuring an over-the-wing distributed-propulsion system and a propulsive empennage. The objective of this study is to understand the sensitivity of the design to different mission requirements, design parameters, and technology assumptions, in order to establish design guidelines for distributed-propulsion aircraft.

The HEP concept, which aims for an entry-into-service year of 2035, is presented in Fig. 1, along with the conventional aircraft configuration used as reference. The hybrid-electric aircraft presents two distinct propulsion systems. The first is a propulsive empennage (PE), which acts as the main source of thrust and is responsible for the control and stability of the aircraft [20]. The second is an over-the-wing distributed-propulsion system, which is attached to the flap mechanism in order to provide thrust vectoring (TV) in low-speed conditions. Although previous design studies of the propulsive-empennage concept indicate that this propulsion system leads to a slightly higher maximum take-off mass (MTOM) than conventional turboprop configurations due to an increased center-of-gravity excursion [20], the combination of this system with over-the-wing (OTW) DP entails multiple benefits. Firstly, the placement and shielding of the propulsors may lead to a reduction in both cabin noise and flyover noise [8]. Secondly, the propulsion-airframe integration challenges in terms of ground clearance are removed, and thus a shorter landing gear is possible. Thirdly, since the total thrust is divided over two propulsion systems, the disk loading of each system can be reduced, effectively leading to an increase in bypass ratio [18] which increases the average propulsive efficiency. And, finally, given that only a fraction of the total power has to be diverted to the DP system, the weight of the electrical powertrain components is limited. In this sense, a fully serial architecture leads to significant weight penalties [21]. The concept in Fig. 1b, on the other hand, presents a series/parallel partial-hybrid architecture. Since the use of batteries is

likely to be detrimental [21], a partial turboelectric (PTE) architecture is a strong alternative. However, given that the SPPH powertrain is the most generic architecture [22], it allows the designer to analyze whether a small amount of batteries is beneficial and, if not, then the optimal result will automatically lead to a PTE architecture.

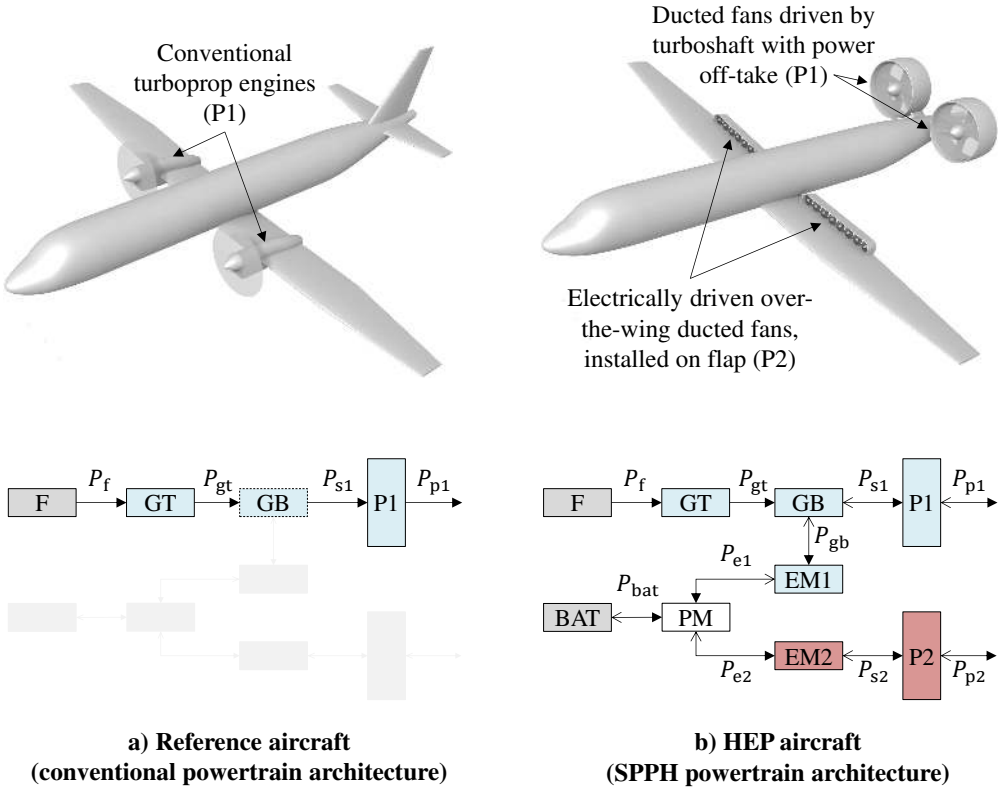

a) Reference aircraft (conventional powertrain architecture)

b) HEP aircraft (SPPH powertrain architecture)

Fig. 1 Notional representation of the reference (left) and HEP (right) aircraft concepts, indicating the external layout of the propulsion systems (top) and associated powertrain architecture (bottom). Legend: "F" = fuel, "GT" gas turbine, "GB" = gearbox, "P" = propulsor, "EM" = electrical machine, "PM" = power management and distribution system, "BAT" = battery, "1" = primary powertrain branch, "2" = secondary powertrain branch.

In addition to the supposed benefits at aircraft level, there are several reasons for analyzing this concept from a research perspective. In first place, the potential benefits of using of DP for thrust-vectoring in tube-and-wing aircraft have not been analyzed sufficiently. Although there are aircraft concepts which make use of this strategy [9], information regarding the direct and indirect effects of TV is scarce. In second place, although the use of over-the-wing DP may entail several aerodynamic benefits [23], no design studies have been found which explicitly include these effects. Due to the multidisciplinary nature of this problem, most design studies assume a constant aerodynamic benefit [1], ignoring the key sensitivities. Therefore, a thorough analysis of the impact of DP at aircraft level would provide insight into possible areas of improvement, and serve as a starting point for more detailed studies on topics such as aerodynamic performance, noise emissions, power management, or control and stability. To this end, the aircraft is sized and evaluated following the methodology described in Sec. II. The resulting design is then compared to the reference aircraft for a series of design parameters, mission requirements, and technology assumptions in Sec. III.

II. Methodology

A brief overview of the sizing method used for both the reference and the HEP aircraft is given in Sec. II.A. In order to incorporate the effects of DP, the aero-propulsive model described in Sec. II.B is used. While the sizing method is applicable to any tube-and-wing aircraft configuration and any set of performance requirements, the aero-propulsive model is specific for propeller aircraft. Finally, Sec. II.C defines the figures of merit used to evaluate the overall performance of the aircraft.

A. Design Procedure

The top-level weight breakdown, installed power, and wing area of the aircraft are computed using the method described in Ref. [22]. This preliminary sizing method modifies the traditional Class-I sizing routines by including the aero-propulsive interaction effects and a simplified HEP-powertrain model. Due the strong aerodynamic coupling between a DP system and the wing, the changes in lift, drag, and propulsive efficiency are computed for over-the-wing DP using the model described in in the following section. For the propulsive empennage and conventional propellers they are neglected, since the aerodynamic coupling is less severe. When these aerodynamic interaction effects are incorporated in the point performance equations of the power-loading diagram and mission analysis of the aircraft, the impact of aero-propulsive interaction on the propulsive-power requirements and energy consumption can be estimated. The propulsive power is in turn related to the power requirements of each component of the powertrain by applying a power balance across each element while assuming a constant transmission or conversion efficiency. This leads to a separate power-loading diagram for each component in the powertrain, based on which the designer must select a design point in terms of wing loading and power loading. During the mission analysis, the powertrain components are automatically re-sized to meet the power demand if the constraint diagram underestimated the power requirements. This may be the case for specific combinations of mission requirements and power-control variables, and implies that the limiting performance criteria (e.g., top-of-climb climb rate) has not been included in the constraint diagram.

In order to determine the complete behavior of the SPPH powertrain architecture, three power-control parameters must be specified: the gas turbine throttle (ξ_{GT}), the supplied power ratio (Φ), and the shaft power ratio (φ). These are, respectively, defined as

$$\xi_{\mathrm{GT}} = \frac{P_{\mathrm{GT}}}{P_{\mathrm{GT,max}}}, \tag{1}$$

$$\Phi = \frac{P_{\mathrm{bat}}}{P_{\mathrm{bat}} + P_{\mathrm{f}}}, \tag{2}$$

$$\varphi = \frac{P_{\mathrm{s2}}}{P_{\mathrm{s2}} + P_{\mathrm{s1}}}. \tag{3}$$

While the gas turbine throttle indicates how much power the gas turbine produces with respect to its maximum capability in a given flight condition, the supplied power ratio describes the power share at the two energy sources. Likewise, the shaft power ratio describes the power share at the two shafts. For a more elaborate description of these variables and their relation to the selected powertrain architecture, the reader is referred to Ref. [22]. For this paper, it is important to note that these three power-control parameters are time-dependent variables, whose profile throughout the mission must be chosen by the designer. The selected values have a direct impact on the aircraft size, since they affect both the constraints in the power-loading diagram, and the energy consumption estimated during the mission analysis. The degree-of-hybridization (of energy) of the aircraft DOH $= E_{\mathrm{bat}}/(E_{\mathrm{bat}} + E_{\mathrm{f}})$, meanwhile, is a scalar result of the sizing process.

The values of the main design variables, assumptions, and requirements are not explicitly discussed here for brevity, but can be found in Appendix A. Nevertheless, for context, the assumptions made regarding the properties of the powertrain components are presented in Table 1. The values of specific energy and specific power assumed for the batteries at pack level are commonly used in design studies for the 2035 timeframe, even though these values are considered optimistic given that they approach the maximum theoretical values attainable with lithium-ion batteries at cell level [25]. For the batteries, a minimum state-of-charge of 20% is maintained. The values of specific power and transmission efficiency assumed for the electrical machines and inverters/rectifiers are based on the state-of-the-art research goals presented in Ref. [26]. Since both the thermal management system and additional elements of the power management and distribution (PMAD) system can constitute a significant weight contribution (see e.g. Refs. [9, 14, 27]), the weight of the electrical systems estimated by the design method—which only includes electromotors, generators, inverters and rectifiers—is increased by 30%. This generic weight penalty is assumed due to a lack of information in the preliminary sizing phase for an accurate estimation of the weight of components such as coolers, transformers, or cables. For this reason, Sec. III.D.1 presents a sensitivity analysis of the assumed component properties. Finally, the thermal efficiency of the gas turbine is assumed to be 0.34 for the reference aircraft. An additional 20% improvement is hypothesized for the 2035 timeframe. Given that the thermal efficiency is kept constant throughout the sizing process, the potential benefit of improved gas turbine performance due to electrical assistance in off-design conditions is not accounted for. The weight of the gas turbines is estimated using the empirical correlation of Ref. [28].

Table 1 Powertrain component properties. Values assumed for 2035 timeframe, unless otherwise stated.

Battery specific energy at pack level [Wh/kg]	500	Gas turbine efficiency (current) [-]	0.34
Battery specific power at pack level [kW/kg]	1	Gas turbine efficiency (2035) [-]	0.40
Specific power of electrical machines [kW/kg]	13	Electrical machine efficiency [-]	0.97
Specific power of converters [kW/kg]	19	Converter efficiency [-]	0.99
Weight penalty for PMAD and cooling elements	30%	PMAD efficiency [-]	0.99
Minimum battery state-of-charge	20%	Gearbox efficiency [-]	0.96

B. Aero-Propulsive Model

Two contributions to lift, drag and propulsive efficiency are considered in the sizing method. The simplified breakdown, which is defined in Ref. [22], can be expressed as

$$C_L = C_{L,\text{airframe}} + \Delta C_L, \tag{4}$$

$$C_D = C_{D,\text{airframe}} + \Delta C_D, \tag{5}$$

$$\eta_\text{p} = \eta_{\text{p,isolated}} + \Delta\eta_\text{p}. \tag{6}$$

The first term of the right-hand side of Eqs. 4–6 corresponds to uninstalled conditions, that is, to the lift and drag of the airframe when no propulsion system is present, and to the propulsive efficiency of the propulsors if these were operating in freestream conditions. In this study, it is assumed that the airframe lift is generated entirely by the wing. For airframe drag, a parabolic lift polar is assumed, i.e. $C_{D,\text{airframe}} = C_{D0,\text{airframe}} + C^2_{L,\text{airframe}}/(\pi Ae)$. Following the traditional Class-I sizing methods [29], a constant propulsive efficiency is assumed per mission segment for the propulsive empennage, since this propulsion system presents no strong aerodynamic interaction effects with the airframe*. For the DP system, on the other hand, it is necessary to estimate the isolated-propulsor efficiency, in order to account for the sensitivity to propulsor diameter. Given that the total disk area scales with the square of the propulsors' diameter but linearly with the number of propulsors, multiple small propulsors have a significantly lower total disk area than a single large fan or propeller for a given span of wing covered. Hence, if the DP system is responsible for a large fraction of the total thrust, high thrust coefficients are obtained, and consequently the propulsive efficiency deteriorates. Therefore, the propulsive efficiency of the DP system in uninstalled conditions is estimated using

$$\eta_{\text{p,isolated}} = \frac{2k_\text{p}}{1 + \sqrt{1 + \dfrac{8T_\text{c}}{\pi}}}, \tag{7}$$

where the thrust coefficient is defined as $T_\text{c} = T_\text{p}/(\rho v^2 D_\text{p}^2)$, and k_p is a correction factor. For $k_\text{p} = 1$, Eq. 7 provides the maximum theoretical efficiency of an actuator disk. Since the propulsive efficiency is in reality lower than predicted by momentum theory due to swirl and viscous losses, $k_\text{p} < 1$. Based on the empirical data presented in Ref. [30], a value of $k_\text{p} = 0.88$ is used in this study.

The second contribution to lift, drag, and propulsive efficiency comprises the changes in uninstalled performance due to aerodynamic interaction between the propulsors and the airframe when these are integrated with each other. These "delta" terms depend on the geometry of the system, and vary with wing lift and propeller thrust. The aero-propulsive model used to estimate these terms is created using the numerical method outlined in Ref. [23]. The method combines a panel method to simulate the wing, a blade-element method adapted to non-uniform inflow, and a vortex-lattice method to compute the velocities induced by the slipstream on the wing. With this method, a single propeller above a high aspect-ratio rectangular wing is simulated. The superposed effect of multiple adjacent propellers is not considered, and the contributions of nacelles and ducts are neglected at this stage. The wing and propeller geometries are based on the wind-tunnel models used to validate the tool, and therefore do not represent an optimized OTW-propeller geometry. Although these simplifications limit the applicability of the model, it is considered accurate enough for the preliminary sizing phase.

*The thrust of the propulsive empennage would, in practice, have a strong effect on trim drag, but preliminary sizing methods do not include this drag term.

The aero-propulsive model is evaluated for a range of thrust coefficients, wing angles-of-attack, and propeller-diameter to wing-chord ratios. The propeller position is kept at $x_p/c = 0.85$, maintaining a fixed blade pitch and a clearance between the propeller disk and the wing surface equal to 1% of the wing chord. For each case, lift, pressure drag, and propulsive efficiency are computed. Based on wind-tunnel observations [23], the change in friction drag on the wing is expected to be small, and is therefore neglected. Six thrust coefficients are evaluated (in the interval $0.01 \leq T_c \leq 0.55$), combined with eleven angle-of-attack values ($0^o \leq \alpha \leq 10^o$) and six diameter-to-chord ratios ($0.2 \leq D_p/c \leq 0.8$), leading to a total of 396 sample points. For each combination of α and D_p/c, a propeller-off simulation is carried out as well, in order to obtain "deltas" with respect to zero-thrust conditions. In order to decrease the runtime of the sizing method, a three-dimensional, fifth-order polynomial fit is applied to the lift and drag data. The polynomial coefficients are obtained using a linear least-squares algorithm, and the coefficient of determination of the resulting fit is verified to be $R^2 > 0.99$ in both cases. While the changes in lift coefficient ΔC_L and drag coefficient ΔC_D present a monotonic dependency on the three input variables, the change in propulsive efficiency $\Delta\eta_p$ presents a non-monotonic dependency on thrust which cannot be accurately predicted with a polynomial fit. Hence, for $\Delta\eta_p$, a two-dimensional, third-order polynomial fit is applied in D/c and α ($R^2 = 0.987$), and the resulting value is interpolated linearly at the corresponding thrust coefficient.

Figure 2 illustrates the changes in lift coefficient, drag coefficient, and propulsive efficiency for two generic thrust coefficients. The lift and drag coefficients are normalized with the wing reference area corresponding to the spanwise interval occupied by a single propeller, $c \cdot D_p$. Figure 2 shows that, at low thrust coefficients, the lift and drag of the

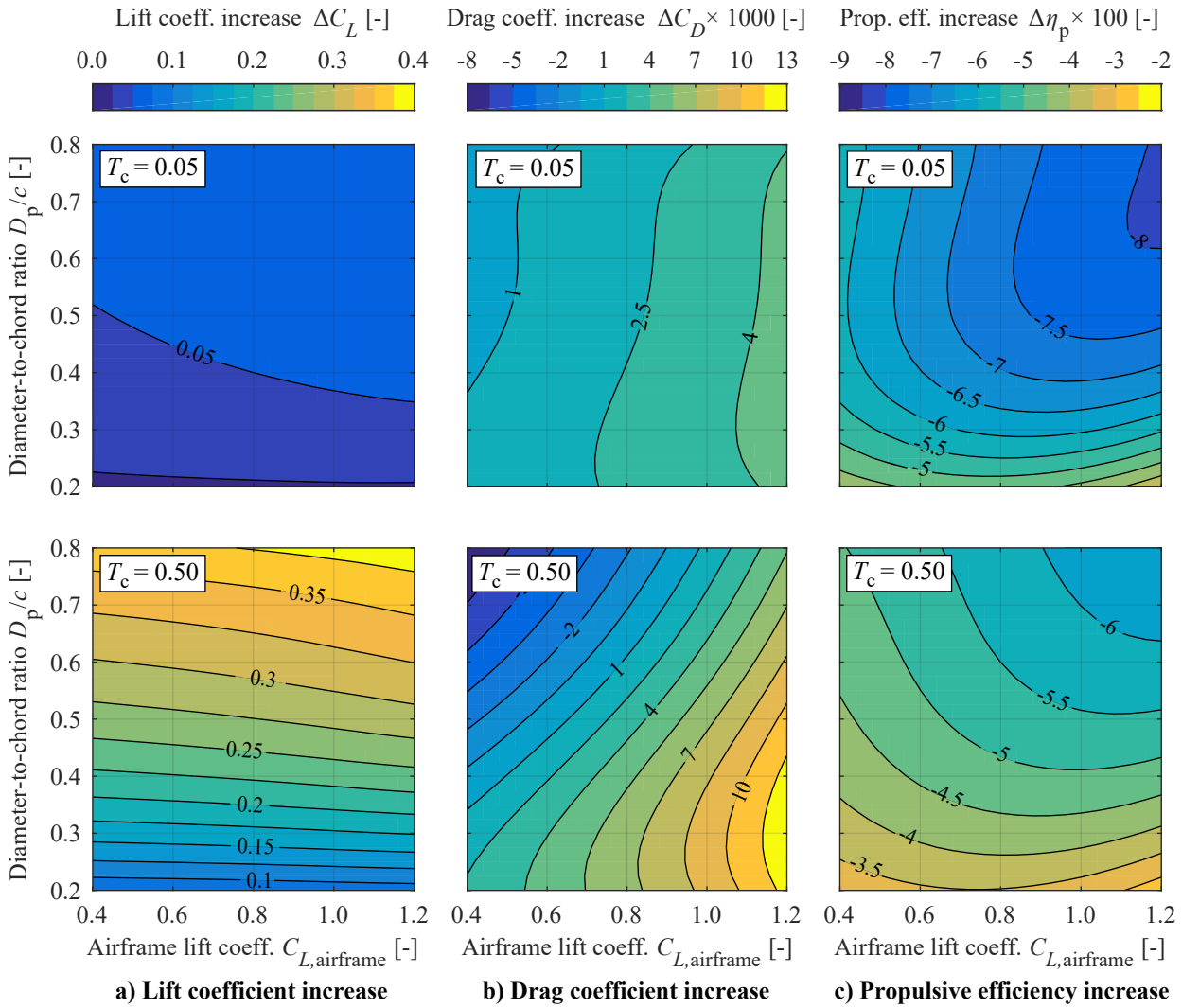

a) Lift coefficient increase **b) Drag coefficient increase** **c) Propulsive efficiency increase**

Fig. 2 From left to right: increase in lift coefficient, drag coefficient and propulsive efficiency due to aero-propulsive interaction effects, estimated by the surrogate model for low (top) and high (bottom) thrust settings.

wing present only a minor increase, while the propulsive efficiency is adversely affected. The propulsive-efficiency penalty increases with increasing wing lift coefficient due to increased supervelocities over the wing. This is partially compensated at low diameter-to-chord ratios due to a change in the effective angle-of-attack experienced by the propeller, leading to a slight increase in propulsive efficiency [23]. The results at higher thrust coefficients show that ΔC_L increases with increasing thrust and diameter-to-chord ratio, while being fairly insensitive to the airframe lift coefficient. The variation in drag, on the other hand, can be either positive or negative, depending on the angle of attack of the wing and the propeller size. For low angles of attack (i.e., low airframe lift coefficients) and high D_p/c values, the drag is reduced due to increased suction on the forwards-facing surface of the suction side of the airfoil. Finally, the propulsive efficiency penalty is lower at high thrust coefficients, since the relative impact of the wing on propeller performance is reduced.

The thrust coefficient and lift-coefficient values for which the aero-propulsive model was generated are representative of the cruise, descent, and (majority of the) climb segments of the mission. However, in low speed conditions (take-off and landing), the required thrust and lift coefficients are higher, and the numerical model is not capable of providing an accurate estimation [23]. In these conditions, ΔC_L, ΔC_D, and $\Delta\eta_\mathrm{p}$ are limited to the values they obtain at the bounds of the surrogate model. This is considered a conservative approach, since the aero-propulsive benefits improve with increasing thrust coefficient. However, some studies indicate that the OTW propeller may adversely affect the maximum lift coefficient on the wing [32]. On the other hand, preliminary wind-tunnel tests suggest that inclining the propulsors for thrust vectoring may further increase lift and decrease drag without an appreciable propulsive efficiency penalty [23]. In general, this shows that there is a large amount of uncertainty regarding the maximum lift coefficient attainable with these systems. For this reason, a separate sensitivity analysis is carried out with respect to the assumed maximum lift coefficient in Sec. III.D.2.

C. Figures of Merit

Two figures of merit are used in this study to quantify the overall performance of the hybrid-electric aircraft. In most cases, these metrics are presented as a percentage change with respect to the reference aircraft. In this way, the areas where a hybrid-electric configuration outperforms conventional architectures can easily be identified. The first figure of merit is the maximum take-off mass (MTOM, or m_TO) of the aircraft. This parameter is often used for comparison in aircraft design studies, since it gives an indication of the "size" of the aircraft and has a direct impact on power requirements, energy requirements, production and maintenance costs, and the certification of the aircraft.

A second figure of merit is required that characterizes the energy consumption of the aircraft, which is tightly related to the costs of the fuel and electricity required to operate the system, as well as its emissions[†]. Several such metrics exist for conventional aircraft, such as the payload-range efficiency (PRE = $W_\mathrm{PL}R/W_\mathrm{f}$) [33], or the payload-fuel energy efficiency (PFEE = $W_\mathrm{PL}R/E_\mathrm{f}$) [34]. Alternative metrics have also been used for hybrid-electric aircraft, such as the energy-specific air range (ESAR = $\mathrm{d}R/\mathrm{d}E$) [35], the cost-specific air range (COSAR) [27], or the productivity-specific energy consumption (PSEC = $E/(m_\mathrm{PL}R)$) [36], where the energy consumed E includes both fuel and battery energy. However, when quantifying the overall "efficiency" of the aircraft in terms of energy consumption, only the energy consumed during the nominal mission must be considered, and not the reserves. Although the reserves affect the MTOM of the aircraft—and therefore, indirectly, the energy consumption—they do not directly define the energy consumed during its day-to-day operation. Given that the metrics found in literature are not directly applicable to hybrid-electric aircraft, do not consider the amount of payload carried, or do not take into account exclusively the energy consumed during the nominal mission, a new definition is proposed. This new figure of merit, the *payload-range energy efficiency*, is an adaption of the existing metrics and can be expressed as

$$\mathrm{PREE} = \frac{W_\mathrm{PL}R}{E_\mathrm{miss}}, \tag{8}$$

that is, as the payload weight times the harmonic range of the aircraft and divided by the total energy consumed during the nominal mission (excluding reserves). This dimensionless parameter represents how many joules of "useful work", interpreted as the work required to displace a unit of payload over a unit of distance, are extracted per joule of energy consumed by the system. Note that this parameter can be larger than one, and should therefore not be interpreted as a thermal or mechanical efficiency η.

[†]If the electrical power used to charge the batteries comes from a renewable energy grid, the fuel consumption may be a more indicative parameter of aircraft emissions than the total energy consumption. However, given the low degrees of hybridization analyzed in this study and the fact that state-of-art electrical power grids obtain energy predominantly from non-renewable energy sources, this distinction is ignored.

III. Results

The results are grouped into four sections. First, in Sec. III.A the conventional configuration is compared to reference aircraft data to verify that the assumed aircraft characteristics are reasonable, and to a baseline HEP variant. The baseline mission requirements correspond to those of a 70-passenger regional turboprop: the aircraft must have a harmonic range of R = 850 nmi with a 7500 kg payload, and a baseline cruise altitude and Mach number of 17,000 ft and 0.41, respectively. Sections III.B, III.C, Sec. III.D then analyze the sensitivity of the HEP design to different design parameters, mission requirements, and technology assumptions, respectively. In some cases, the optimum found in a sensitivity analysis is taken as starting point for subsequent analyses. Although this does not provide the optimum design, it ensures that insight is provided in the more relevant parts of the design space.

A. Baseline Design

Table 2 collects several top-level parameters of the conventional aircraft configuration and the baseline HEP configuration. Details regarding the selected design-parameter values and performance requirements can be found in Appendix A. The conventional configuration with current technology assumptions is compared to reference data of an ATR 72-600. The MTOM is underestimated by 2.5%, while the fuel energy is overestimated by 7%. These two characteristics are reduced by 6% and 23%, respectively, when evaluating the 2035-configuration. In this variant, only two modifications have been assumed. Firstly, the thermal efficiency of the gas turbine has been increased (see Table 1). Secondly, the design point corresponding to maximum wing loading has been selected, instead of a trade-off between maximum wing loading and maximum power loading, as reflected in Fig. 3a. This allows a fair comparison between the conventional and HEP architectures, since the point of maximum wing-loading led to an improved design, as discussed in Sec. III.B.1. In the following sections, the conventional architecture evaluated for the 2035 timeframe will be taken as the reference aircraft for comparison with the HEP variant.

Table 2 Summary of sizing results, comparing two conventional configurations and the baseline HEP configuration. Lift-to-drag ratio is presented as cruise-phase average. Fuel and battery energy include reserves.

	ATR 72-600 (Ref. [37])	**Conventional (current)**	**Conventional (2035)**	**Baseline HEP**
Take-off mass, m_{TO} [t]	22.8	22.2	20.9	24.1
Wing loading, W_{TO}/S [kN/m^2]	3.67	3.64	4.00	4.50
GT power loading, $W_{TO}/P_{GT,max,SL}$ [N/kW]	58.2	54.6	49.7	49.5
Wing area, S [m^2]	61.0	59.8	51.3	52.6
Fuel energy, E_f [GJ]	85.6	91.7	70.2	84.6
Battery energy, E_{bat} [GJ]	0	0	0	1.1
Cruise lift-to-drag ratio, $(L/D)_{cr}$ [-]	-	17.3	17.9	18.4
Payload-range energy efficiency [-]	-	2.02	2.11	1.77

The design parameters selected for the baseline HEP concept are chosen manually without any prior knowledge of the optimal values. For the selected power-control variables (whose values can be found in Appendix A), the battery provides additional power during take-off. As a consequence, the power requirement for the gas turbine is reduced, and the take-off constraint is no longer its sizing constraint, as reflected in Fig. 3b. However, both the primary electrical machines (generators) and secondary electrical machines (electromotors) are sized for take-off conditions. Note that the one-engine-inoperative constraints do not influence the secondary electrical machines, since a total of 10 electromotors are used, and thus the failure of one of these elements does not constitute a limitation to the remaining nine. Furthermore, the maximum wing loading of the HEP concept is increased due to thrust vectoring and aero-propulsive interaction in landing conditions. Consequently, it presents a small increase in cruise lift-to-drag ratio when compared to the reference aircraft, as shown in Table 2. Nevertheless, the hybrid-electric configuration is outperformed by the reference aircraft in terms of both MTOM and energy consumption. The main reasons for this are the increased weight due to the hybrid-electric powertrain components, and the reduced propulsive efficiency of the OTW propulsors in cruise conditions.

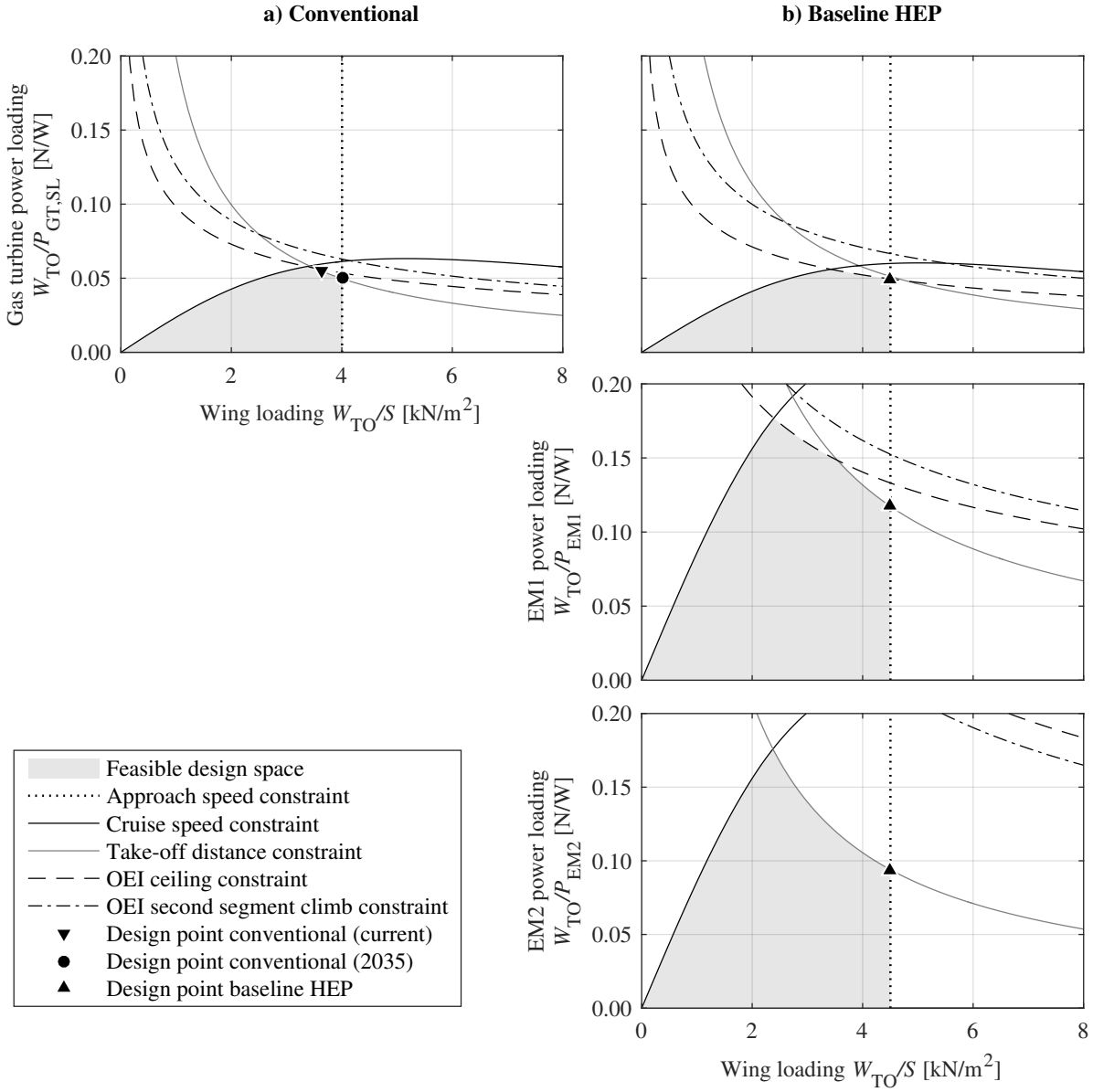

Fig. 3 Power-loading constraint diagrams of the conventional (left) and baseline HEP (right) configurations.

B. Sensitivity to Design Parameters

1. Design Point Selection

In the preliminary sizing process, the designer must choose a design point in the power-loading diagram. Due to the large weight contribution of the powertrain to MTOM in the case of HEP, a priori it was hypothesized that the design point for maximum power loading might lead to a lighter aircraft than the design point for maximum wing loading. This is, however, not the case, as shown in Fig. 4a. This figure shows that the top-right corner of the design space leads to the lightest aircraft. The point of maximum (gas turbine) power loading can be misleading in this sense, since the associated wing-loading value corresponds to a minimum gas-turbine size per unit weight of the aircraft, but not to the minimum electrical-machine size, as visible in Fig. 3b.

For this aircraft, the point of minimum MTOM also corresponds to the point of maximum payload-range energy efficiency. The contours of PREE shown in Fig. 4 are more skewed than the MTOM contour lines, indicating that this parameter is relatively more sensitive to wing loading. This is a result of the direct effect of wing loading on aerodynamic efficiency and, consequently, on energy consumption. Although this design point has been identified as the optimal one in design studies of comparable HEP configurations as well [31], this is evidently not always the case for hybrid-electric aircraft [38].

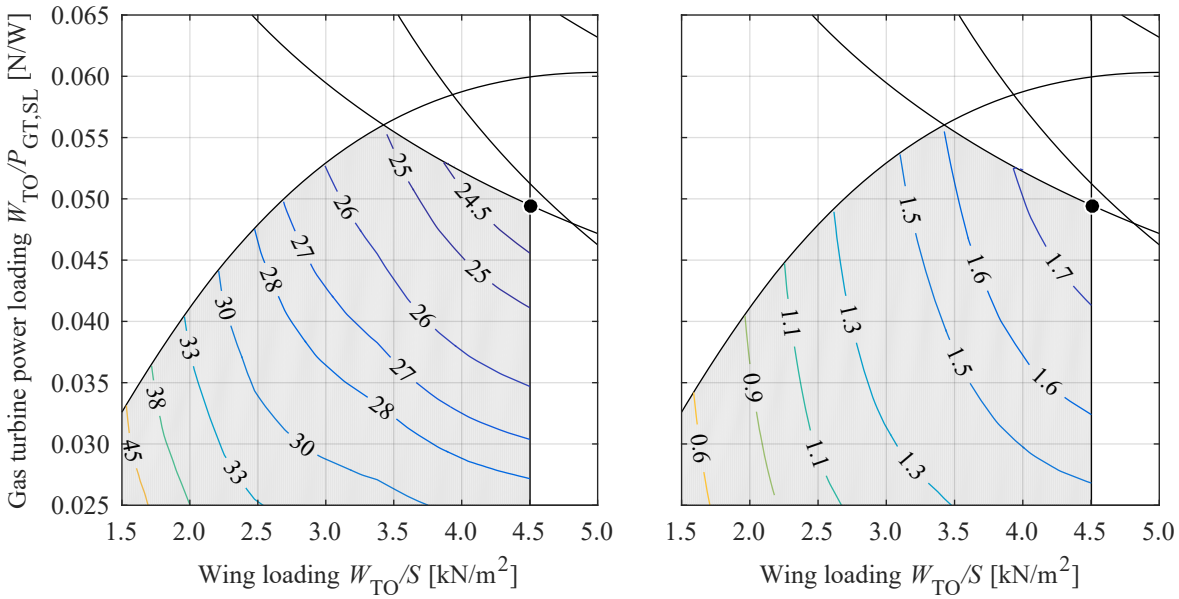

a) MTOM contours **b) PREE contours**

Fig. 4 Gas-turbine power-loading diagram of the HEP concept, showing the feasible design space in gray together with contour lines of constant MTOM (left; values expressed in metric tons) and payload-range energy efficiency (right). The marker indicates the selected design point.

2. Distributed-Propulsion System Design Parameters

When designing an aircraft with distributed propulsion, some of the key parameters which must be selected are the number of DP-propulsors and their size. Since no clear design guidelines have been found in this regard, Fig. 5 presents the sensitivity of MTOM and PREE to the number of propulsors N, and the wing span-fraction covered ΔY—which, together with N, determines the size of each propulsor. The figures of merit are presented as a percentage change with respect to the reference aircraft. The minor fluctuations visible in the bottom-right corner of the plots are attributed to the discontinuities in propulsor size, since N must be an integer.

From Fig. 5 it is evident that, within the intervals analyzed, the HEP concept is heavier and less efficient than the reference aircraft for all combinations of N and ΔY. However, this penalty is severely increased for large values of N combined with low values of ΔY, that is, for small propulsor sizes. For the baseline HEP concept, a shaft power ratio of $\varphi = 0.5$ is selected in all flight conditions except landing, and thus approximately half of the total thrust has to be distributed over a small total disk area in these conditions. This is detrimental for the isolated propulsors' efficiency, as indicated by Eq. 7. A reduction in propulsive efficiency is detrimental for energy consumption in cruise, but also has a large negative impact on powertrain weight in take-off conditions, where the electrical components are sized (see Fig. 3). Therefore, the results of Fig. 5 are not only dependent on the aero-propulsive model, but also on the selected power-control strategy. In any case, this figure highlights the importance of estimating the propulsive efficiency in the design process, instead of assuming a constant value. It is worth adding that, even though the bottom-right corner of Fig. 5 may seem beneficial, in practice this would lead to very large over-the-wing propulsors, which entails other drawbacks to which the preliminary-sizing phase is not sensitive.

A second characteristic of the DP system which is to be explored is the use of thrust vectoring. To this end, Fig. 6 shows the changes in MTOM and PREE obtained when varying the TV angle in take-off and landing. For all other flight phases, the angle is zero. Again, the HEP configuration presents a weight and PREE penalty for all combinations sampled. However, an improvement with respect to the baseline is possible. The contour plots show a minimum MTOM around $\alpha_{p,TO} = 10^o$, $\alpha_{p,L} = 55^o$. During take-off, a small degree of thrust vectoring is beneficial to enhance lift, although larger deflections are detrimental, since the axial component of thrust is reduced. During landing, on the other hand, larger deflections lead to a lighter and more efficient aircraft. As $\alpha_{p,L}$ increases, so does the wing loading of the aircraft, and consequently the lift-to-drag ratio L/D in cruise is improved. However, for $\alpha_{p,L} > 55^o$, two things

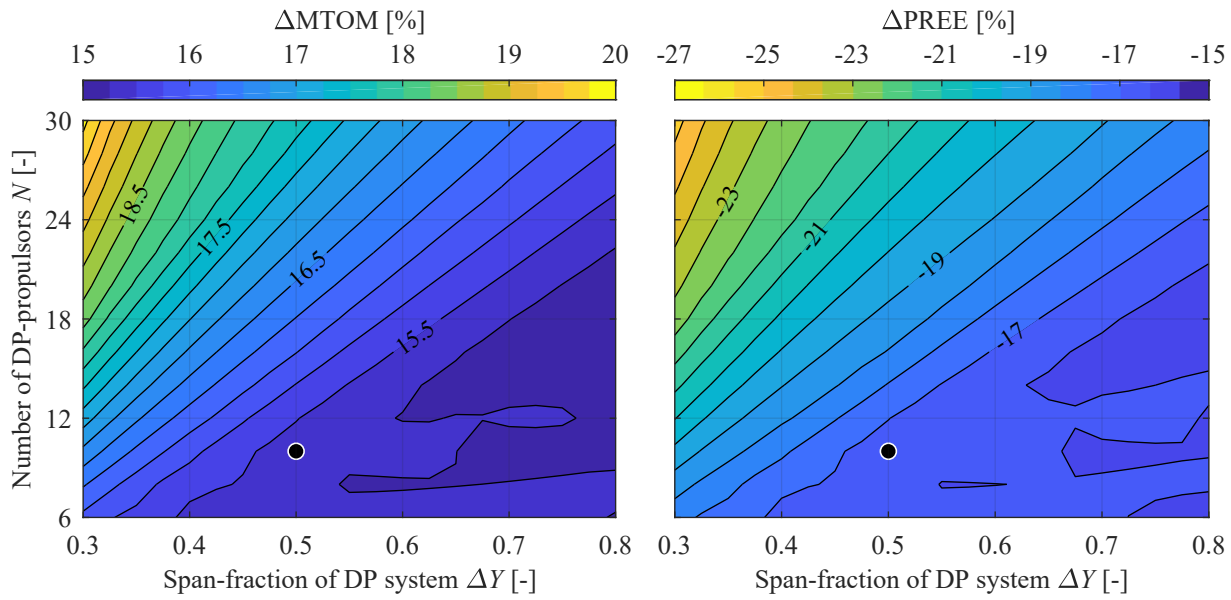

a) MTOM change w.r.t. reference **b) PREE change w.r.t. reference**

Fig. 5 Change in MTOM (left) and PREE (right) with respect to the reference aircraft, as a function of the number of propulsors and wing span-fraction occupied by the DP system. The marker indicates values used for the baseline design.

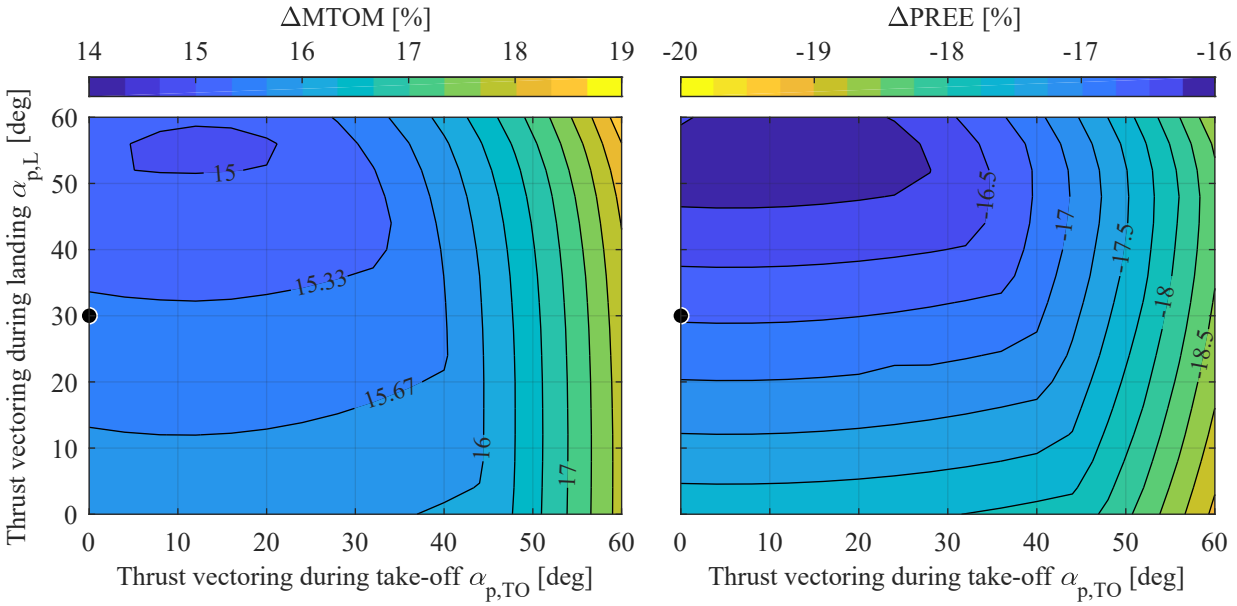

a) MTOM change w.r.t. reference **b) PREE change w.r.t. reference**

Fig. 6 Change in MTOM (left) and PREE (right) with respect to the reference aircraft, as a function of the thrust-vectoring angle employed during take-off and landing. The marker indicates values used for the baseline design.

occur. Firstly, the wing area is reduced so much that the lift coefficient in cruise approaches, and then exceeds, the value corresponding to maximum L/D, thus decreasing the overall aircraft performance. This key consideration has to be taken into account when sizing a DP system, and will be discussed in more detail in the following sections. Secondly, the wing loading surpasses the intersection of the OEI-ceiling constraint with the take-off constraint in the gas-turbine power-loading diagram, and thus the weight of the gas turbine increases more rapidly with increasing wing loading. This can be seen in the constraint curves of Fig. 3b for $W_{TO}/S > 4.5$ kN/m^2. The same effect is responsible for the discontinuity in gradient at, e.g., $(\alpha_{p,TO}; \alpha_{p,L}) = (40; 23)$: as the thrust-vectoring angle during take-off is increased past its optimum for a given $\alpha_{p,L}$, the take-off constraint descends in the gas-turbine power-loading diagram and starts limiting the size of the gas turbine.

3. Power-Control Strategy

For the first stages of the sizing process, the designer must choose a set of power-control parameters. Given the relatively large amount of design variables, and the fact that—as suggested in the previous section—these variables can have a decisive impact on the aircraft's design, an optimization could be the way forward. However, since the objective of this study is to understand the effect of the different variables, a design-of-experiments (DOE) is performed. For the SPPH architecture, three power-control parameters (Eqs. 1–3) have to be specified per performance constraint. For each of the six mission segments (climb, cruise, and descent of the nominal mission, plus diversion), a linear evolution of the these control parameters is assumed. Since in cruise conditions one of them has to remain free in order to satisfy the flight condition, this leads to a total of 49 variables. By assuming the same profiles for the nominal mission and the diversion, using the same strategy during take-off and second-segment climb, and fixing the gas-turbine throttle for determined flight phases (maximum throttle in take-off, engine-idle in descent, etc.), the number of variables is reduced to 19. A latin-hypercube sampling technique is used to distribute 15,000 sample points in the design space. An upper and lower bound are imposed on each variable, in order to avoid energy harvesting ($\varphi < 0$ or $\varphi > 1$) or samples which are known to lead to poor results (e.g., a large supplied power ratio during cruise). The values of these bounds can be found in Appendix A.

The results of the DOE in terms of MTOM and PREE are collected in Fig. 7a, with the colormap indicating the degree-of-hybridization (of energy) the design. Figure 7a confirms three characteristics of HEP aircraft. Firstly, the

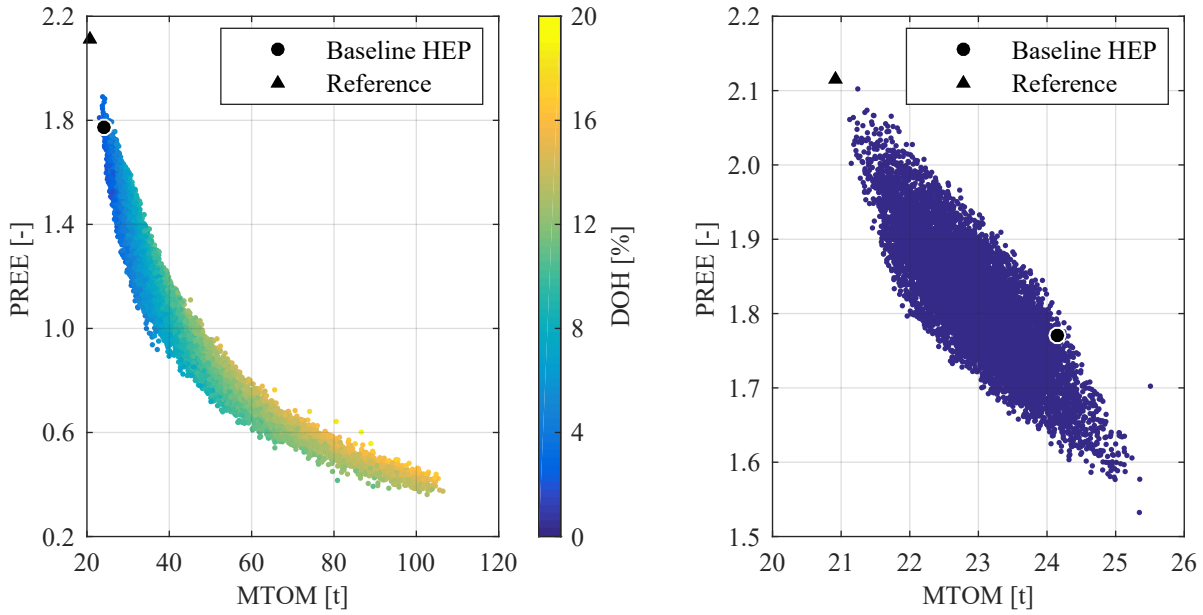

a) Original HEP configuration (SPPH) **b) $\Phi = 0$ (PTE)**

Fig. 7 Results obtained from the power-control-parameter DOE carried out for the baseline HEP concept (left), together with the results obtained when the supplied power ratio is set to zero for all constraints and mission segments (right).

power-control strategy is a driving factor in the design process, since a bad strategy may significantly over-size the aircraft (over 100 tons, in this case). Secondly, for a given PREE, the MTOM increases as the DOH increases. In other words, if the objective of a design is to minimize in-flight emissions, for example, then a slightly heavier aircraft carrying additional battery energy may be more beneficial. And thirdly, a lower DOH (i.e., low Φ values) leads to a lighter and more energy-efficient aircraft, as expected for the technology levels assumed. Inspection of the optimal point in terms of PREE revealed a similar strategy to the baseline configuration: the batteries are used during take-off and climb, and are charged during descent in order to keep enough energy in the batteries for a second take-off and climb in case of a diversion. Although this allows for a smaller gas turbine and a more efficient well-to-shaft energy transmission, the battery weight penalty outweighs these benefits. In a strict sense, however, this is not a fair comparison, since the potential benefit of improved gas-turbine efficiency through on-design sizing is not accounted for.

Based on the previous observations, a second DOE was carried out. In this case, all Φ values were set to zero, meaning that in essence a partial-turboelectric architecture was simulated. The results of this second DOE are plotted in Fig. 7b. As can be seen from the range of the axes, the MTOM and PREE obtained in this case are of the same order as the reference aircraft, although the HEP concept still performs worse than the reference even in the most ideal scenario. It is also evident that, while Fig. 7a suggests that the control variables were appropriately selected for the baseline configuration, Fig. 7b shows that there is still room for improvement. In order to understand the main reasons for these differences, Fig. 8 presents the control-variable values corresponding to the optimum point in terms of PREE for both DOE's. The most notable difference between the baseline strategy and the improved strategy obtained for the PTE case is a reduction of the shaft power ratio, especially in take-off and cruise. Although the DP system increases the lift-to-drag ratio for a given wing loading, it leads to an appreciable propulsive-efficiency penalty (see Fig. 2). Furthermore, additional power is lost when converting the shaft power of the gas turbine to electrical power, distributing it along the airframe, and converting it back to mechanical power. Thus, in theory, distributed propulsion can improve propulsive efficiency through a decrease in disk loading [18], but this benefit can easily be counteracted by propulsive-efficiency penalties due to non-uniform inflow and losses in the components of the electrical system. For this reason, Fig. 8 suggests that the propulsive empennage should remain as the main source of thrust for all mission segments except during landing ($\varphi \approx 1$). In landing conditions, a large fraction of the total thrust should be diverted to the DP system, in order to enhance wing lift and provide an additional vertical force through thrust vectoring. However, the total thrust during landing is generally low, since the aircraft must maintain its approach speed. Consequently, the powertrain components are not sized by power requirements during landing, and thus ξ_{GT} and Φ were not varied in the DOE.

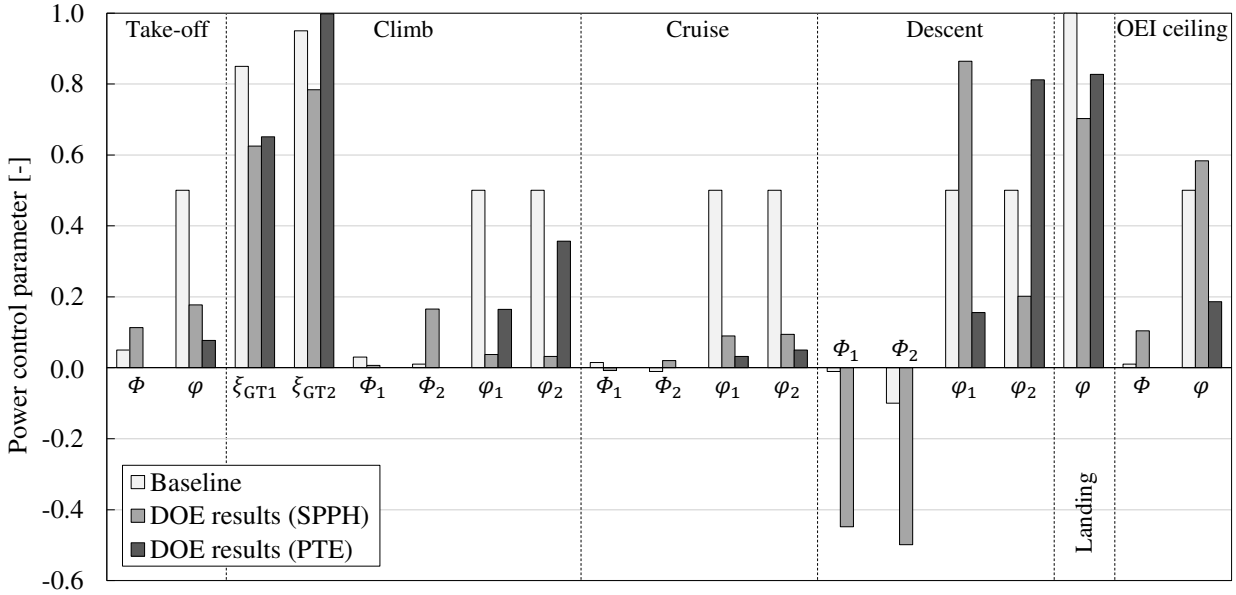

Fig. 8 Comparison of between power-control parameter values used for the baseline HEP design and the ones corresponding to maximum PREE in the two design-of-experiments.

C. Sensitivity to Mission Requirements

In this section, the performance of the HEP configuration is evaluated for a range of payload weights, harmonic ranges, and cruise Mach numbers. A distinction is made between evaluating the mission requirements at fixed altitude and at optimum altitude, in order to illustrate the importance of this design consideration. Two Mach numbers are considered: the cruise Mach number of the ATR 72 ($M_{cr} = 0.41$), and a "high-speed" case ($M_{cr} = 0.6$). For this sensitivity study, the best power-control strategy identified in the previous section is applied (i.e., no batteries are employed). Thus, during cruise, most thrust is generated by the propulsive empennage, and the propulsive efficiency is nearly constant. Furthermore, based on the findings of Sec. III.B.2, thrust vectoring angles of 10^o and 55^o are used in take-off and landing, respectively.

1. Sensitivity at a Fixed Cruise Altitude

Figure 9 presents the results of the payload–range sweep at the original cruise altitude of 17,000 ft. For each payload–range combination, ΔMTOM and ΔPREE are computed based on a HEP aircraft and a conventional aircraft which are both sized for the given mission requirements. Note that at $M_{cr} = 0.6$ the sizing routine does not converge for $R = 400$ nmi, since the climb and descent phases exceed the nominal mission range. The same occurs for $R > 1750$ nmi, in this case because the powertrain is heavily over-sized, and consequently the aircraft presents a positive excess power during part of the descent phase, with the engine in idle conditions ($\xi_{GT} = 0.1$). This problem could be mitigated by changing the power-control variables, but it is considered preferable to obtain the trends without an additional variation of these variables.

With the newly selected design parameters, the HEP configuration presents a minor weight increase and PREE reduction for the baseline mission ($M_{cr} = 0.41$, Figs. 9a and Figs. 9b). However, the PREE improves with increasing range and, to a lesser extent, with increasing payload. The trend of PREE with range is attributed to an increased lift-to-drag ratio in cruise of the HEP configuration ($(L/D)_{cr} \approx 18.4$) when compared to the reference aircraft ($(L/D)_{cr} \approx 17.7$). At $M_{cr} = 0.6$ (Figs. 9c and 9d), the PREE gain is increased to nearly 12% with respect to the reference aircraft, and the sensitivity of MTOM to mission range is larger than for the $M_{cr} = 0.41$ case. The flaw of this analysis becomes evident when comparing the lift-to-drag ratio of the reference and hybrid-electric aircraft, which attain values of approximately 10.9 and 12.6, respectively. The L/D benefit of the HEP configuration is larger in this case, and thus the sensitivity of ΔMTOM with respect to range increases. However, these L/D values clearly show that the combination of cruise altitude and Mach number are not adequate for the selected wing loading. In these conditions, the lift coefficient is significantly lower than the value corresponding to optimum L/D.

2. Sensitivity at Optimal Cruise Altitude

The payload–range maps are also evaluated at 45 equally spaced flight levels between 12,000 ft and 34,000 ft. The lower bound is equal to the OEI ceiling, while the upper bound corresponds to a typical cruise altitude for turbofan aircraft. For each payload–range combination, the optimum altitude in terms of PREE is selected for each aircraft. Thus, the two configurations are not necessarily sized at the same altitude. In this case, the results differ in trend and in value from the ones obtained at constant altitude, as can be observed in Fig. 10.

Figures 10a and 10b show that, at $M_{cr} = 0.41$, the hybrid-electric variant is approximately 2.5% heavier than the reference, and presents a 2.5% lower payload-range energy efficiency. For the conventional configuration, the optimum cruise altitude increases from 19,000 ft at short harmonic ranges, to 24,000 ft at long harmonic ranges. For the HEP aircraft, the optimum cruise altitude increases from 15,000 ft at short harmonic ranges, to 20,000 ft at long harmonic ranges. The optimum altitude increases with harmonic range, because the efficiency gain during cruise offsets the increase in energy required to climb to that altitude. In general, the hybrid-electric aircraft has a lower optimum altitude than the reference, due to the increased wing loading enabled by DP. At their optimum altitude, both aircraft configurations have a comparable lift-to-drag ratio. Therefore, the fact that the PREE and MTOM penalties of the HEP configuration reduce with decreasing range is attributed its lower cruise altitude. For example, at 400 nmi range, the optimum cruise altitude of the HEP configuration is 4,000 ft lower than the conventional configuration, and thus it requires less energy for climbing.

At $M_{cr} = 0.6$, the upper altitude bound was identified as optimum for both the reference and the HEP aircraft. At this flight speed, the weight and PREE penalties of the hybrid-electric configuration are greater than for $M_{cr} = 0.41$. Surprisingly, the weight penalty is minimized for high payloads and short ranges, while the PREE penalty is minimized for high payloads and high ranges. In this case, the lift-to-drag ratio of the reference aircraft is approximately 17.7, while for the HEP variant it is approximately 18.3. Based on these L/D values, it appears that the HEP configuration

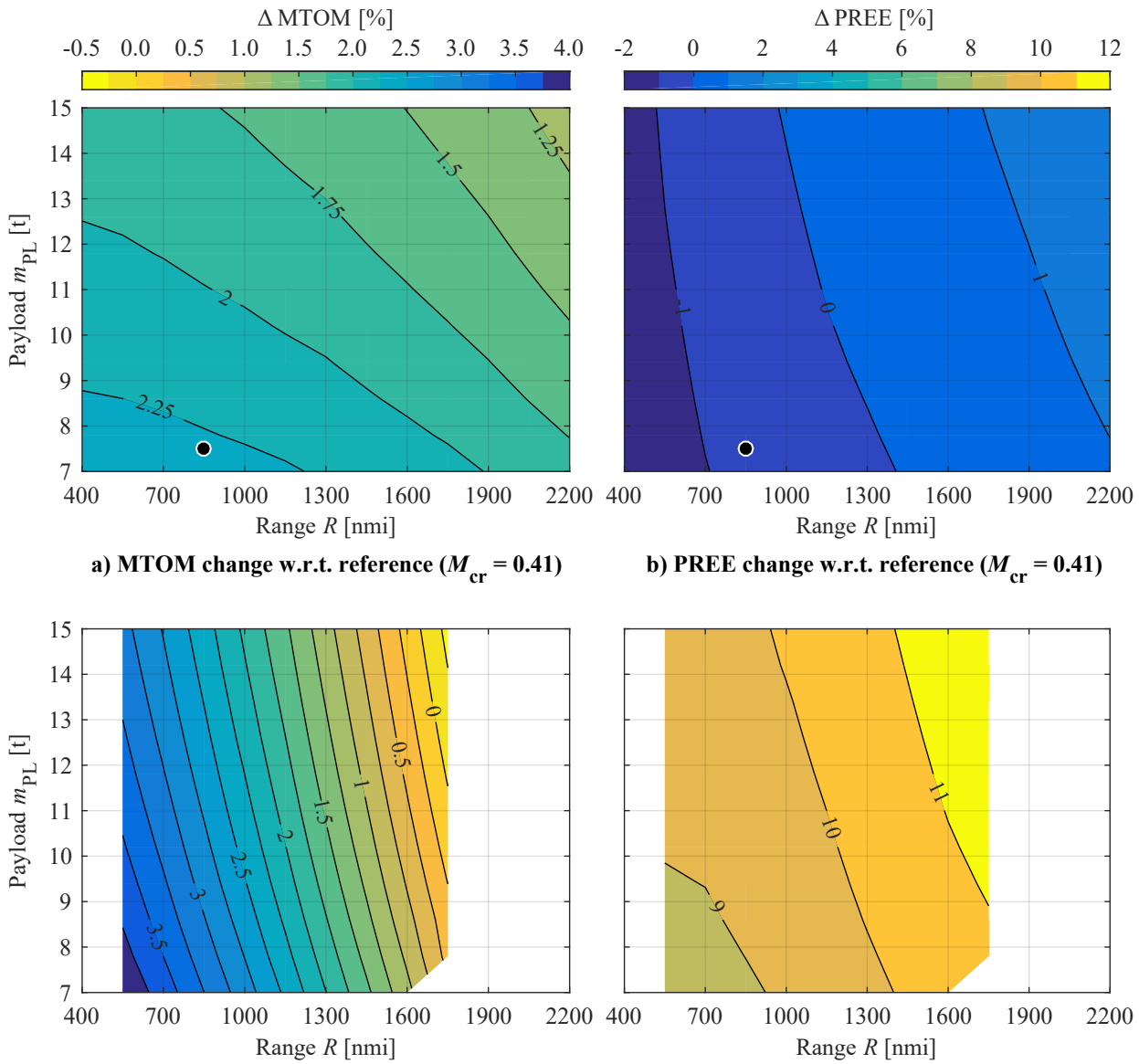

a) MTOM change w.r.t. reference (M_{cr} = 0.41)

b) PREE change w.r.t. reference (M_{cr} = 0.41)

c) MTOM change w.r.t. reference (M_{cr} = 0.60)

d) PREE change w.r.t. reference (M_{cr} = 0.60)

Fig. 9 Change in MTOM (left) and PREE (right) of the PTE configuration with respect to the reference aircraft, for different payload, range, and cruise Mach number requirements. All missions are performed with a cruise altitude of 17,000 ft. The marker indicates values used for the baseline design.

operates near its optimum altitude, and for this reason, ΔPREE improves with increasing range. On one hand, this indicates that additional altitudes must be evaluated for a fair comparison. On the other, this also shows that, if the cruise altitude of the aircraft is restricted by air traffic regulations or other requirements, the use of HEP provides an additional degree-of-freedom which can be used to tailor the wing loading such that an optimal L/D is achieved in cruise.

The main characteristics of the improved HEP design, evaluated for the baseline mission (m_{PL} = 7500 kg, R = 850 nmi, M_{cr} = 0.41) at optimum altitude, are summarized in Table 3. Additional variables can be found in Appendix A. The results show a significant improvement with respect to the baseline design in all aspects except power loading, which is decreased. However, the HEP configuration is still outperformed by the reference aircraft, which is also evaluated at its optimum altitude.

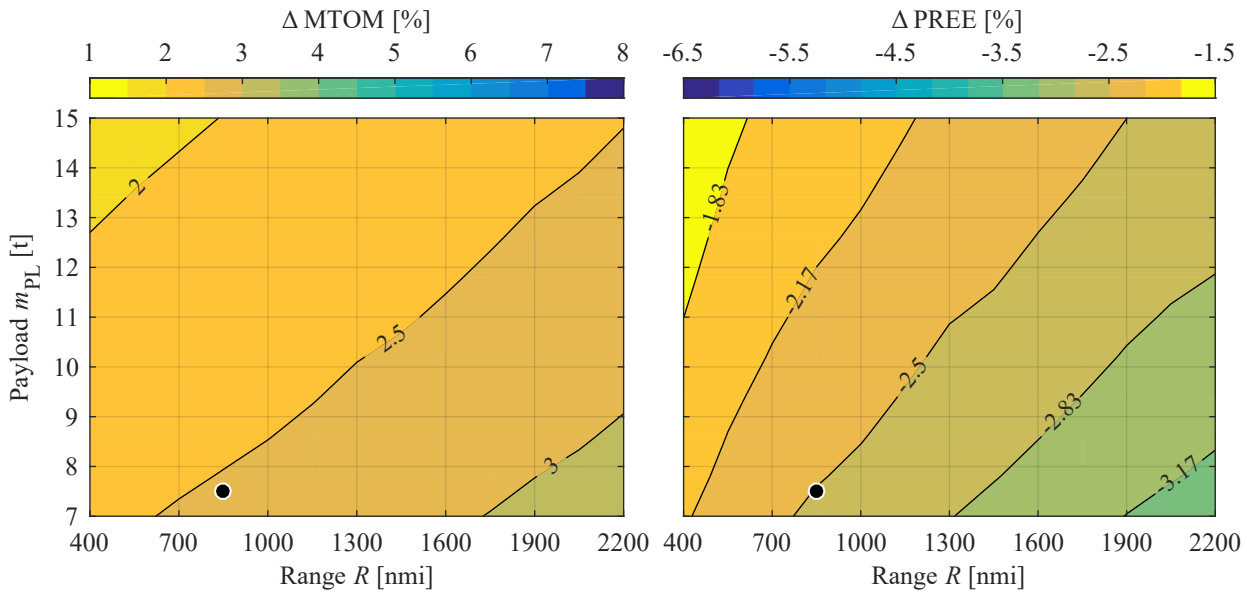

a) MTOM change w.r.t. reference (M_{cr} = 0.41) **b) PREE change w.r.t. reference (M_{cr} = 0.41)**

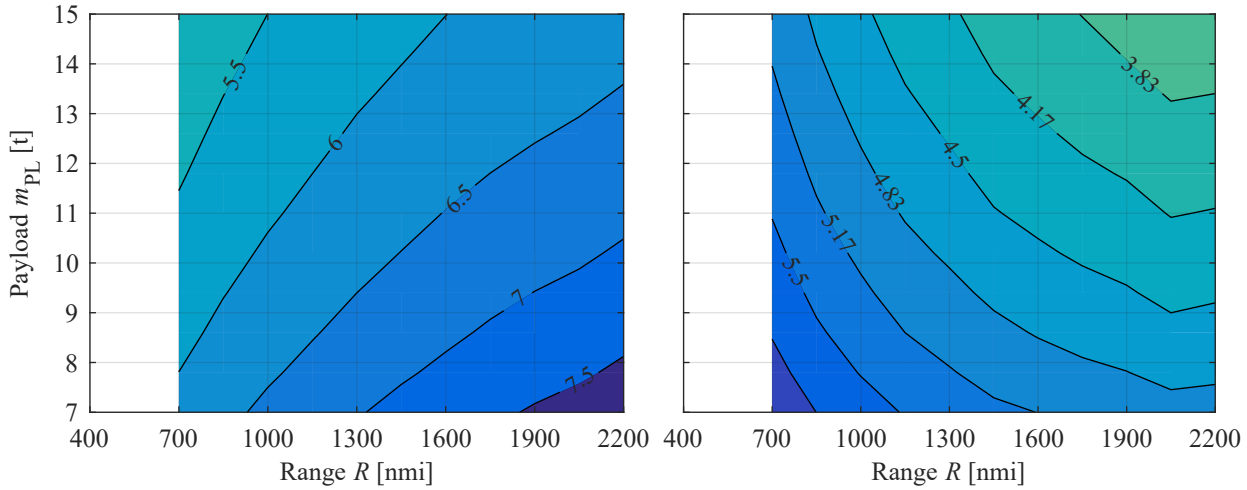

c) MTOM change w.r.t. reference (M_{cr} = 0.60) **d) PREE change w.r.t. reference (M_{cr} = 0.60)**

Fig. 10 Change in MTOM (left) and PREE (right) of the PTE configuration with respect to the reference aircraft, for different payload, range, and cruise Mach number requirements. All missions are performed at optimum cruise altitude. The marker indicates values used for the baseline design (at a different cruise altitude).

D. Sensitivity to Technology Assumptions

1. Powertrain Component Technology Levels

The results of Sec. III.B.3 show that the use of batteries is detrimental for both figures of merit for the assumed mission and aircraft layout. In order to assess whether this conclusion is highly dependent on the battery's characteristics, Fig. 11 presents the sensitivity of MTOM and PREE to the specific energy and specific power of the batteries at pack level. Both properties are varied between 50% and 300% of the baseline value reported in Table 1. For this assessment, the baseline SPPH configuration was used. As expected, an improvement in battery technology leads to an appreciable reduction in MTOM and increase in PREE. However, even for the optimistic values of 3 kW/kg and 1500 Wh/kg, the concept performs worse than the one without batteries. For the baseline case, the battery mass is sized by power

Table 3 Main characteristics of the improved HEP design, evaluated for the baseline mission at optimum cruise altitude. Lift-to-drag ratio is presented as cruise-phase average. Fuel and battery energy include reserves.

		Difference w.r.t. baseline HEP	Difference w.r.t. reference
Take-off mass, m_{TO} [t]	21.4	-11.4%	+2.5%
Wing loading, W_{TO}/S [kN/m^2]	4.70	+4.4%	+17.4%
Gas turbine power loading, $W_{TO}/P_{GT,SL}$ [N/W]	0.043	-13.1%	-13.5%
Wing area, S [m^2]	44.7	-15.1%	-12.6%
Fuel energy, E_f [GJ]	71.5	-15.4%	+3.3%
Battery energy, E_{bat} [GJ]	0	-100%	0%
Cruise altitude, h_{cr} [ft]	18,000	+5.9%	-16.3%
Cruise lift-to-drag ratio, $(L/D)_{cr}$ [-]	18.4	+0.2%	+0.2%
Payload-range energy efficiency [-]	2.10	+18.5%	-2.5%

requirements, hence being insensitive to the assumed specific energy. In the top-left corners of Fig. 11, on the other hand, the battery mass is sized by energy requirements, and is therefore insensitive to specific power. The curve defined by the loci points on the response map that present a discontinuity in gradient (i.e, at the kink of the contour lines) delimits these two regions. The location of this limit depends on the chosen power-control strategy. Modifying the power-control strategy such that the design point ends up on this discontinuity means that the full potential of the battery is used in terms of both energy and power. Logically, this simple distinction is an artifact of assuming constant battery properties at pack level. For a more accurate result, a battery model is required. With an appropriate design of the battery, the trade-off between energy requirements and power requirement can be tailored for the specific design, and in that case the response maps would no longer present these two clearly distinguishable regions.

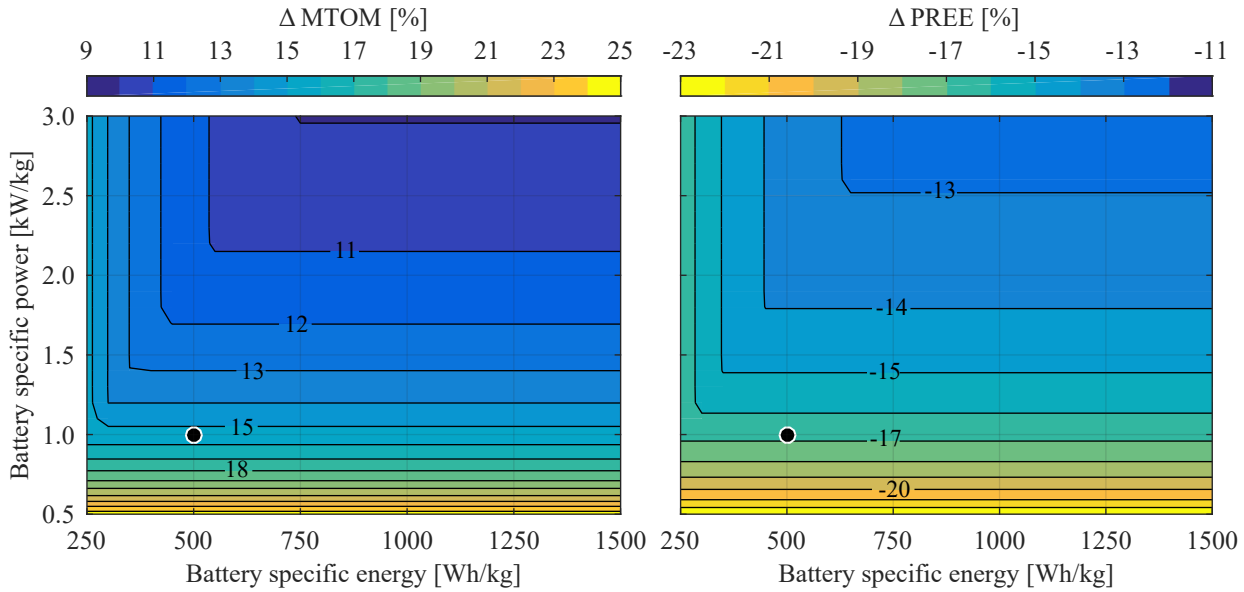

a) MTOM change w.r.t. reference **b) PREE change w.r.t. reference**

Fig. 11 Change in MTOM (left) and PREE (right) of the baseline SPPH concept with respect to the reference aircraft, as a function of the specific energy and specific power of the batteries at pack level. The marker indicates values used for the baseline design.

In second place, the sensitivity of MTOM and PREE to the weight and efficiency of the electrical components of the powertrain (excluding batteries) is assessed. Since this comprises multiple elements (electrical machines, converters, and additional PMAD components), the specific power and efficiency of these elements is varied simultaneously. In order to provide the sensitivity at a relevant point in the design space, the PTE configuration obtained from the DOE is analyzed. For illustration purposes, a *combined specific power* (CSP) is defined for the PTE architecture as

$$\mathrm{CSP} = \sum_{i=1}^{n} \frac{1}{(1/\mathrm{SP}_i)}, \tag{9}$$

where n is the number electrical components through which the power flows, and SP_i the specific power of the component i. For example, for the baseline case, $\mathrm{CSP} = (1/1.3) \cdot (1/19 + 1/13 + 1/13 + 1/19)^{-1} = 2.97$ kW/kg. For simplicity, the CSP can be interpreted as the power produced by the electrical system divided by the total electrical-system weight[‡]. Analogously, a chain efficiency is defined as the product of efficiencies of all the components in the electrical system, which in the simplified PTE model are connected in series. For example, the baseline chain efficiency is $\eta_{\mathrm{EM}}^2 \cdot \eta_{\mathrm{converter}}^2 \cdot \eta_{\mathrm{PMAD}} = 0.91$. In other words, an overall improvement in the technology levels of the electrical powertrain components is simulated by simultaneously improving all components by an equal amount, and is quantified altogether using the CSP and chain efficiency.

The resulting sensitivities are reflected in Fig. 12. Although both MTOM and PREE improve with increasing CSP or chain efficiency, PREE is more sensitive to the latter than MTOM is. In baseline conditions, the HEP aircraft presents a MTOM and PREE comparable to the reference, since this analysis is carried out at the original cruise altitude. The PREE benefit increases up to 6% if the CSP of the system is tripled, and the losses approach zero. In these conditions, the MTOM of the HEP aircraft is also 4% lower than the reference aircraft.

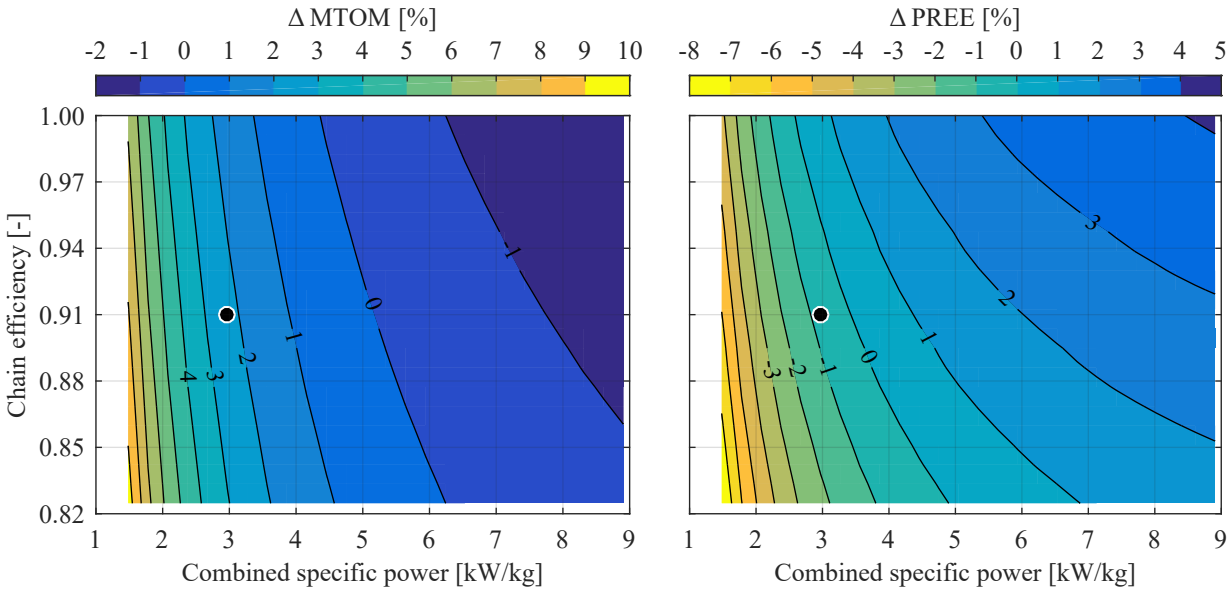

a) MTOM change w.r.t. reference **b) PREE change w.r.t. reference**

Fig. 12 Change in MTOM (left) and PREE (right) of the PTE concept with respect to the reference aircraft, as a function of the combined specific power and efficiency of the electrical powertrain components. The marker indicates values used for the baseline design.

[‡]This is not exactly true, since power is lost in each component, and thus the downstream element transmits a slightly different amount of power. However, since in this case no battery power is added to the system and all efficiencies are $\eta \approx 1$, this inconsistency is negligible for the discussion at hand.

2. Low-Speed Aerodynamic Performance

The performance predictions of the aero-propulsive model are incorrect in low-speed conditions, as discussed in Sec. II.B. To analyze what impact this has on the aircraft, Fig. 13 presents the change in MTOM and PREE as a function of the increase in maximum-lift coefficient due to aero-propulsive interaction, in take-off and landing conditions. This figure shows that the lift benefit during take-off is small in baseline conditions, since the shaft-power ratio during take-off is low (see Fig. 8). Two discontinuities in gradient can also be seen in Fig. 13. When increasing $\Delta C_{L\text{max,TO}}$ at constant $\Delta C_{L\text{max,L}}$, the take-off constraint rises in the gas-turbine power-loading diagram until, at the first discontinuity, it stops limiting the gas-turbine size. If $\Delta C_{L\text{max,TO}}$ is further increased, eventually the total shaft power required from the propulsive empennage starts being limited by the OEI second-segment climb constraint instead of the take-off constraint, leading to the second discontinuity. A more counterintuitive observation in Fig. 13, however, is that an increase in $C_{L\text{max}}$ generally does not improve the design. The reason for this is that, based on the findings of Sec. III.B.2, the PTE configuration already employs TV angles which lead to an optimal wing loading. In this case, if for example $\Delta C_{L\text{max,L}}$ is increased significantly, the lift-to-drag ratio in cruise may increase slightly due to increased wing loading, but the gas-turbine power-loading is reduced, and consequently the aircraft weight increases. From this it can be concluded that, as long as the TV system is capable of producing enough vertical force, the enhancement of $C_{L\text{max}}$ due to aero-propulsive interaction affects the optimum TV angle, but does not directly benefit the design. If, however, the thrust-vectoring angle is limited by, for example, structural or stability constraints, then an increase in $C_{L\text{max}}$ can be beneficial.

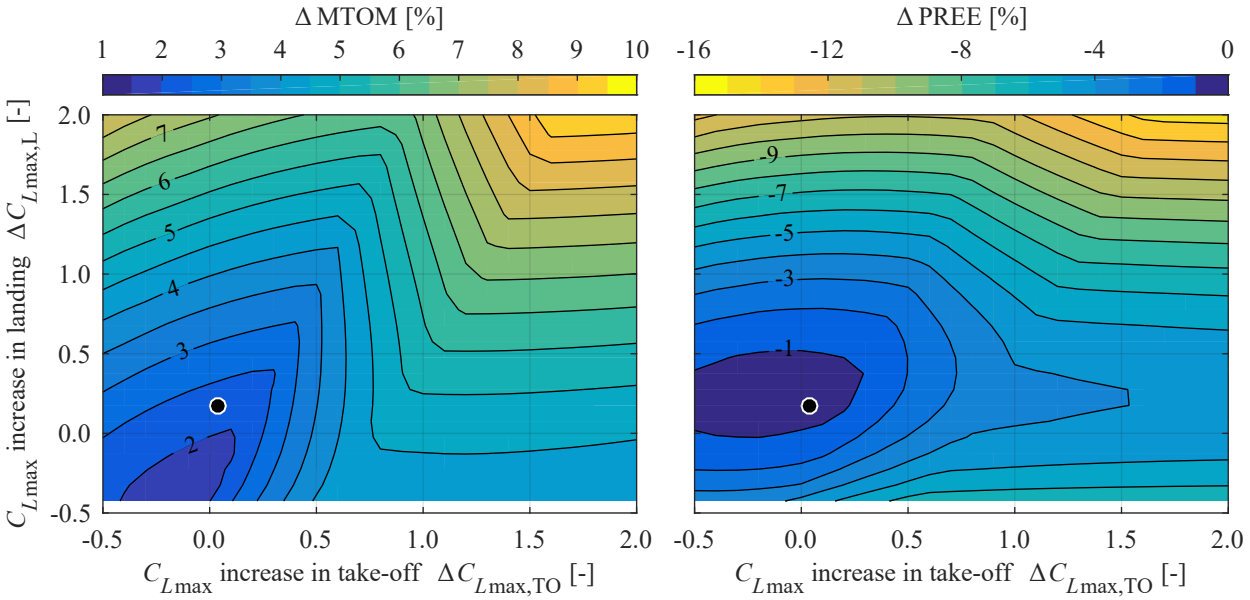

a) MTOM change w.r.t. reference **b) PREE change w.r.t. reference**

Fig. 13 Change in MTOM (left) and PREE (right) of the PTE configuration with respect to the reference aircraft, as a function of the increase in maximum lift coefficient due to thrust in take-off and landing conditions. $\Delta C_{L\text{max}}$ does not include the effect of thrust vectoring. The marker indicates values obtained for the baseline PTE design.

It should be noted that the drag coefficient in low-speed conditions can also have an appreciable impact on the design. During take-off, a decrease in drag would lead to a reduction of the required take-off power, which sizes most components. During landing, an increase in drag would increase the thrust required to maintain a determined approach speed. This would, in turn, increase ΔC_L and the effect of thrust vectoring, and therefore the maximum wing loading would be increased. However, the take-off constraint is evaluated using the take-off parameter [28], which is not sensitive to the drag coefficient. The effect of an increase in maximum wing loading, on the other hand, is already evident in Fig. 13. Hence, no sensitivity study was carried out with respect to the drag coefficient in low speed conditions.

IV. Discussion & Conclusions

In this study, a preliminary sizing method has been used to analyze the sensitivity of a hybrid-electric aircraft configuration to a series of design parameters, mission requirements, and technology assumptions. Although literature suggests that hybrid-electric propulsion (HEP) can lead to significant improvements in terms of energy consumption and environmental impact, the results evidence that several theoretical benefits at subsystem level do not necessarily lead to an improvement at aircraft level when the relevant dependencies are included in the sizing process. As an example, the payload-range energy efficiency of the best HEP configuration proposed in this study is still 2.5% lower than a conventional aircraft. Nevertheless, several important conclusions can be drawn based on the sensitivity analyses.

In first place, when designing a hybrid-electric aircraft, it must be compared to a conventional configuration sized for the same mission, and each concept must be evaluated at its optimum cruise altitude. Not doing so can lead to an overestimation of the HEP aircraft's benefits. In this study, a comparison at constant cruise altitude suggests that the HEP aircraft can present up to a 12% increase in payload-range energy efficiency. In cruise conditions, the optimal lift coefficient $C_L = (W/S)/(0.5\rho v^2)$ is determined by the drag polar, and hence there is a trade-off between altitude ($\rho = f(h)$) and wing loading for a given Mach-number requirement. Since W_{TO}/S is directly proportional to the maximum effective lift coefficient during landing, with distributed-propulsion (DP) it is easy to fine-tune the wing loading to its optimal value. In addition to a modification of the high lift devices, DP systems can increase the maximum lift through aero-propulsive interaction or by means of thrust vectoring. However, these efforts are in vain if the conventional configuration can attain an equally efficient C_L in cruise by varying its altitude. In spite of this, there are at least three circumstances under which the increase in wing-loading enabled by DP may still be beneficial. The first occurs when the cruise altitude is fixed by, for example, air traffic regulations. The second corresponds to short harmonic ranges, when an appreciable amount of energy is consumed during the climb segment. In that case, the lower optimal altitude of the HEP aircraft is beneficial. And thirdly, when the maximum wingspan is limited by airport constraints, a HEP aircraft can carry more payload or employ a higher aspect-ratio wing. Furthermore, for the same aspect ratio and bending-relief effects, a smaller wing is less heavy.

The second main finding is related to the performance of the DP-system in cruise conditions. Previous studies indicated that, for the same wing loading and flight condition, DP can still provide a benefit through a reduction in disk loading or an increase in wing lift-to-drag ratio. However, the results show that the propulsive-efficiency penalty due to non-uniform inflow and the losses in the electrical powertrain components outweigh these benefits. This illustrates how an incorrect modeling of the aero-propulsive effects or an overestimation of the powertrain component efficiencies can lead to erroneous conclusions. In addition to this, sensitivity of the DP system's performance to design parameters such as the number of propulsors must be incorporated from the beginning of the sizing process, to avoid an over-prediction of the propulsive efficiency.

In third place, the sensitivity studies confirm that the power-control strategy has a large impact on both the constraint diagram and the mission analysis, and therefore affects practically all characteristics of the aircraft. The optimal control strategy is also highly dependent on the aero-propulsive interaction effects. For example, the design-of-experiments has shown that a low shaft power ratio (i.e., low thrust share of the DP-system) is better in cruise, due to the propulsive-efficiency penalty of the DP system. However, if this penalty could be reduced by properly re-designing the over-the-wing propulsors, then it may be more beneficial to maximize the shaft power ratio in cruise. For this, the improvement in lift-to-drag ratio and propulsive efficiency must exceed the losses in the powertrain components. Given that the chain efficiency of the powertrain's electrical components is 91% in this study, a small improvement in propulsive efficiency would not have a noticeable impact at aircraft level, since the DP system is not used in cruise. If, on the other hand, the propulsive efficiency increases sufficiently to offset this 9% penalty, then suddenly the design would become sensitive to its value. In that case, the increase in aero-propulsive efficiency would not only affect the optimal control strategy, but also the optimum mission. This interconnection between different aspects of the sizing process highlights the importance of analyzing the power-control strategy early in the design process.

Based on these findings, it becomes evident that the proposed concept can only constitute a competitive alternative if several components are improved. Most importantly, the propulsive efficiency of the DP-system must be increased by correctly designing the distributed-propulsion system. Given that the current aero-propulsive model is based on a single over-the-wing propeller with fixed blade pitch, it is likely that the propulsive efficiency can be significantly improved by modifying the blade design and pitch. Furthermore, an optimization of the wing profile and the incorporation of a duct could further improve system performance. Based on the payload–range sweeps, it appears that a concept featuring such a propulsion system could present appreciable advantages for higher payloads, and possibly for longer ranges. Furthermore, the noise emissions must be assessed, to verify whether this configuration could indeed present a low-noise alternative to conventional turboprop aircraft in the future.

Acknowledgments

This research is part of the European Union's Horizon 2020 Clean Sky 2 Large Passenger Aircraft program (CS2-LPA-GAM-2014-2015-01). The authors would like to thank Pepijn Marcus and Martijn Roelofs for helping with the development of the aero-propulsive model, and the NOVAIR project participants for their valuable feedback. Wing, tail and fuselage CAD geometries were created using Pacelab APD 6.0.

References

[1] Sgueglia, A., Schmollgruber, P., Bartoli, N., Atinault, O., Benard, E., and Morlier, J., "Exploration and Sizing of a Large Passenger Aircraft with Distributed Ducted Electric Fans," 2018 AIAA Aerospace Sciences Meeting, Kissimmee, FL, USA, January 8-12 2018. doi:10.2514/6.2018-1745.

[2] Stoll, A. M., and Mikić, G. V., "Design Studies of Thin-Haul Commuter Aircraft with Distributed Electric Propulsion," 16th AIAA Aviation Technology, Integration, and Operations Conference, Washington, DC, USA, June 13-17 2016. doi: 10.2514/6.2016-3765.

[3] Antcliff, K. R., and Capristan, F. M., "Conceptual Design of the Parallel Electric-Gas Architecture with Synergistic Utilization Scheme (PEGASUS) Concept," 17th AIAA/ISSMO Multidisciplinary Analysis and Optimization Conference, Denver, CO, USA, June 5-9 2017. doi:10.2514/6.2017-4001.

[4] Fefermann, Y., Maury, C., Level, C., Zarati, K., Salanne, J. P., Pornet, C., Thoraval, B., and Isikveren, A. T., "Hybrid-Electric Motive Power Systems for Commuter Transport Applicatons," 30th Congress of the International Council of the Aeronautical Sciences, Daejeon, Korea, September 25-30 2016.

[5] Kim, H. D., "Distributed Propulsion Vehicles," 27th Congress of the International Council of the Aeronautical Sciences, Nice, France, September 19-24 2010.

[6] Borer, N. K., Patterson, M. D., Viken, J. K., Moore, M. D., Clarke, S., Redifer, M. E., Christie, R. J., Stoll, A. M., Dubois, A., Bevirt, J. B., Gibson, A. R., Foster, T. J., and Osterkamp, P. G., "Design and Performance of the NASA SCEPTOR Distributed Electric Propulsion Flight Demonstrator," 16th AIAA Aviation Technology, Integration, and Operations Conference, Washington, DC, USA, June 13-17 2016. doi:10.2514/6.2016-3920.

[7] Wick, A. T., Hooker, J. R., Hardin, C. J., and Zeune, C. H., "Integrated Aerodynamic Benefits of Distributed Propulsion," 53rd AIAA Aerospace Sciences Meeting, Kissimmee, FL, USA, January 5-9 2015.

[8] Broadbent, E. G., "Noise shielding for aircraft," *Progress In Aerospace Sciences*, Vol. 17, 1977, pp. 231–268.

[9] Schiltgen, B., Freeman, J. L., and Hall, D. W., "Aeropropulsive Interaction and Thermal System Integration within the ECO-150: A Turboelectric Distributed Propulsion Airliner with Conventional Electric Machines," 16th AIAA Aviation Technology, Integration and Operations Conference, Washington, DC, USA, June 13-17 2016. doi:10.2514/6.2016-4064.

[10] Nguyen, E., Alazard, D., Pastor, P., and Döll, C., "Towards an Aircraft with Reduced Lateral Static Stability Using Electric Differential Thrust," 18th AIAA Aviation Technology, Integration, and Operations Conference, Atlanta, GA, USA, June 25-29 2018.

[11] Kreimeier, M., and Stumpf, E., "Benefit evaluation of hybrid electric propulsion concepts for CS-23 aircraft," *CEAS Aeronautical Journal*, Vol. 8, 2017, pp. 691–704. doi:10.1007/s13272-017-0269-9.

[12] Wroblewski, G. E., and Ansell, P. J., "Mission Analysis and Emissions for Conventional and Hybrid-Electric Commercial Transport Aircraft," 2018 AIAA Aerospace Sciences Meeting, Kissimmee, FL, USA, January 8-12 2018. doi:10.2514/6.2018-2028.

[13] Voskuijl, M., van Bogaert, J., and Rao, A. G., "Analysis and design of hybrid electric regional turboprop aircraft," *CEAS Aeronautical Journal*, Vol. 9, 2018, pp. 15–25. doi:10.1007/s13272-017-0272-1.

[14] Pornet, C., and Isikveren, A. T., "Conceptual design of hybrid-electric transport aircraft," *Progress in Aerospace Sciences*, Vol. 79, 2015, pp. 114–135. doi:10.1016/j.paerosci.2015.09.002.

[15] Isikveren, A. T., Pornet, C., Vratny, P. C., and Schmidt, M., "Optimization of Commercial Aircraft Using Battery-Based Voltaic-Joule/Brayton Propulsion," *Journal of Aircraft*, Vol. 54(1), 2017, pp. 246–261. doi:10.2514/1.C033885.

[16] Bradley, M. K., and Droney, C. K., "Subsonic Ultra Green Aircraft Research Phase II: N+4 Advanced Concept Development," NASA/CR-2012-217556 Technical Report, 2012.

[17] Gladin, J. C., Trawick, D., Mavris, D., Armstrong, M., Bevis, D., and Klein, K., "Fundamentals of Parallel Hybrid Turbofan Mission Analysis with Application to the Electrically Variable Engine," 2018 AIAA/IEEE Electric Aircraft Technologies Symposium, Cincinnati, OH, USA, July 9-11 2018.

[18] Felder, J. L., Kim, H. D., and Brown, G. V., "Turboelectric Distributed Propulsion Engine Cycle Analysis for Hybrid-Wing-Body Aircraft," 47th AIAA Aerospace Sciences Meeting, Orlando, FL, USA, January 5-8 2009. doi:10.2514/6.2009-1132.

[19] National Academies of Sciences, Engineering, and Medicine, *Commercial Aircraft Propulsion and Energy Systems Research: Reducing Global Carbon Emissions*, National Academies Press, 2016. doi:10.17226/23490.

[20] Vos, R., and Hoogreef, M. F. M., "System-level assessment of tail-mounted propellers for regional aircraft," 31st International Congress of the Aeronautical Sciences, Anchorage, Belo Horizonte, Brazil, September 09-14 2018.

[21] Hoogreef, M. F. M., Vos, R., de Vries, R., and Veldhuis, L. L. M., "Conceptual Assessment of Hybrid Electric Aircraft with Distributed Propulsion and Boosted Turbofans," 2019 AIAA Aerospace Sciences Meeting, San Diego, CA, USA, January 7-11 2019.

[22] de Vries, R., Brown, M. T. H., and Vos, R., "A Preliminary Sizing Method for Hybrid-Electric Aircraft Including Aero-Propulsive Interaction Effects," 18th AIAA Aviation Technology, Integration, and Operations Conference, Atlanta, GA, USA, June 25-29 2018.

[23] Marcus, E. A. P., de Vries, R., Raju Kulkarni, A., and Veldhuis, L. L. M., "Aerodynamic Investigation of an Over-the-Wing Propeller for Distributed Propulsion," 2018 AIAA Aerospace Sciences Meeting, Kissimmee, FL, USA, January 8-12 2018.

[24] European Aviation Safety Agency, "Certification Specifications and Acceptable Means of Compliance for Large Aeroplanes," CS-25/Amendment 21, 2018.

[25] Gerssen-Gondelach, S. J., and Faaij, A. P. C., "Performance of batteries for electric vehicles on short and longer term," *Journal of Power Sources*, Vol. 212, 2012, pp. 111–129. doi:10.1016/j.jpowsour.2012.03.085.

[26] Jansen, R. H., Bowman, C., Jankovsky, A., Dyson, R., and Felder, J., "Overview of NASA Electrified Aircraft Propulsion Research for Large Subsonic Transports," 53rd AIAA/SAE/ASEE Joint Propulsion Conference, Atlanta, GA, USA, July 10-12 2017. doi:10.2514/6.2017-4701.

[27] Pornet, C., "Conceptual Design Methods for Sizing and Performance of Hybrid-Electric Transport Aircraft," PhD Dissertation, Technical University of Munich, 2018.

[28] Raymer, D. P., *Aircraft design: A conceptual approach*, AIAA Education Series, 2002. doi:10.2514/4.869112.

[29] Roskam, J., *Airplane Design*, DARcorporation, 1985.

[30] Filippone, A., *Advanced aircraft flight performance*, Cambridge University Press, 2012.

[31] Zamboni, J., Vos, R., Emeneth, M., and Schneegans, A., "A Method for the Conceptual Design of Hybrid Electric Aircraft," 2019 AIAA Aerospace Sciences Meeting, San Diego, CA, USA, January 7-11 2019.

[32] Müller, L., Friedrichs, J., and Kožulović, D., "Unsteady Flow Simulations of an Over-the-wing Propeller Configuration," 50th AIAA/ASME/SAE/ASEE Joint Propulsion Conference, Cleveland, OH, USA, July 28-30 2014.

[33] Nangia, R. K., "Efficiency parameters for modern commercial aircraft," *The Aeronautical Journal*, Vol. 110(1110), 2006, pp. 495–510.

[34] Hileman, J. I., Katz, J. B., Mantilla, J. G., and Fleming, G., "Payload fuel energy efficiency as a metric for aviation environmental performance," 26th International Congress of the Aeronautical Sciences, Anchorage, AK, USA, September 14-19 2008.

[35] Seitz, A., Schmitz, O., Isikveren, A. T., and Hornung, M., "Electrically powered propulsion: Comparison and contrast to gas turbines," Deutscher Luft-und Raumfahrt Kongress, Berlin, Germany, September 2012.

[36] Kruger, M., Byahut, S., Uranga, A., Dowdle, A., Gonzalez, J., and Hall, D. K., "Electrified Aircraft Trade-Space Exploration," 2018 Aviation Technology, Integration, and Operations Conference, Atlanta, GA, USA, June 25-29 2018. doi:10.2514/6.2018-4227.

[37] IHS, "Jane's All the World's Aircraft," , accessed August 2018. URL `https://janes.ihs.com`.

[38] Finger, D. F., Braun, C., and Bil, C., "An Initial Sizing Methodology for Hybrid-Electric Light Aircraft," 2018 Aviation Technology, Integration, and Operations Conference, Atlanta, GA, USA, June 25-29 2018. doi:10.2514/6.2018-4229.

Appendix A: Aircraft Characteristics

Table A.1 Baseline aircraft requirements.

Parameter	Value
Payload, m_{PL} [kg]	7,500
Cruise altitude, h_{cr} [ft]	17,000
Cruise Mach number, M_{cr} [-]	0.41
Range, R [nmi]	825
Take-off field length [m]	1333
Approach speed [kts]	115
OEI ceiling [ft]	12,000
OEI s. s. climb gradient [-]	0.024
Diversion altitude [ft]	10,000
Diversion Mach number [-]	0.3
Diversion range [nmi]	250

Table A.2 Baseline design-parameter values. Asterisks indicate parameters which are only applicable to the hybrid-electric configuration.

Parameter	Value
Aspect ratio, A [-]	12
Half-chord sweep [deg]	0
Taper ratio [-]	0.62
Root thickness-to-chord ratio [-]	0.18
N^o of primary propulsors, N_1 [-]	2
N^o of secondary propulsors*, N_2 [-]	10
DP span fraction*, ΔY [-]	0.5
Spacing between DP propulsors* [-]	0.01
Axial position of DP propulsors*, x_p/c [-]	0.85

Table A.3 Baseline aerodynamic and mission properties assumed per constraint. All parameters are non-dimensional. Asterisks indicate parameters which are only applicable to the hybrid-electric configuration.

	Cruise speed	Approach speed	Take-off distance	OEI ceiling	OEI s. s. climb
Flap configuration	clean	landing	take-off	clean	take-off
Landing gear position	retracted	extended	extended	retracted	retracted
Zero-lift drag coefficient, C_{D_0}	0.022	0.087	0.037	0.022	0.027
Oswald factor, e	0.8	0.95	0.9	0.8	0.9
Maximum lift coefficient, $C_{L_{\text{max,airframe}}}$	-	3	2.1	1.6	2.1
Propulsive efficiency (primary), η_{p1}	0.85	0.8	0.7	0.8	0.75
Aircraft weight fraction	0.98	0.95	1	0.98	1
Gas turbine throttle, ξ_{GT}	0.8	0.5	1	1	1
Supplied power ratio*, Φ	0.01	0.01	0.05	0.1	0.05
Shaft power ratio*, φ	0.5	1	0.5	0.5	0.5

Table A.4 Values of the power-control parameters varied during the DOE. From left to right: baseline value, lower bound in DOE, upper bound in DOE, and the "optimum" value found in the DOE in terms of payload-range energy efficiency. Subscripts "1" and "2" indicate start and end of mission segment, respectively.

		Baseline	Lower bound	Upper bound	Best value
Take-off	Φ	0.05	0	0.5	0
	φ	0.5	0	1	0.032
Climb	ξ_{GT1}	0.85	0.5	1	0.651
	ξ_{GT2}	0.95	0.5	1	0.998
	Φ_1	0.03	0	0.5	0
	Φ_2	0.01	0	0.5	0
	φ_1	0.5	0	1	0.165
	φ_2	0.5	0	1	0.357
Cruise	Φ_1	0.015	-0.05	0.05	0
	Φ_2	-0.01	-0.05	0.05	0
	φ_1	0.5	0	1	0.032
	φ_2	0.5	0	1	0.050
Descent	Φ_1	-0.01	-0.5	0.05	0
	Φ_2	-0.1	-0.5	0.05	0
	φ_1	0.5	0	1	0.160
	φ_2	0.5	0	1	0.811
Landing	φ	1	0	1	0.827
OEI ceiling	Φ	0.01	0	0.5	0
	φ	0.5	0	1	0.187

Table A.5 Main characteristics of the reference aircraft (conventional configuration, 2035 timeframe), the reference aircraft evaluated at optimum altitude, the baseline HEP aircraft, and the improved HEP aircraft evaluated at optimum altitude. Powertrain properties refer to the total installed power or mass, not per component instance.

	Reference (2035)	**Reference (2035, opt. h_{cr})**	**HEP (baseline)**	**HEP (improved, opt. h_{cr})**
Take-off mass [t]	20.9	20.9	24.1	21.1
Operative empty mass [t]	11.8	11.8	14.1	12.0
Wing mass [t]	1.69	1.64	1.89	1.55
Gas turbine mass [t]	1.14	1.14	1.30	1.31
Generator mass [t]	0	0	0.16	0.11
Rectifier mass [t]	0	0	0.11	0.07
Electromotor mass [t]	0	0	0.19	0.10
Inverter mass [t]	0	0	0.13	0.07
Additional PMAD mass [t]	0	0	0.18	0.11
Fuel mass [t]	1.64	1.62	1.98	1.65
Batery mass [t]	0	0	0.61	0
Wing loading [kN/m^2]	4.00	4.00	4.50	4.68
Wing area [m^2]	51.3	51.1	52.6	44.3
Gas turbine power loading [N/kW]	49.7	49.7	49.5	43.1
Generator power loading [N/kW]	N/A	N/A	117.4	148.5
Electromotor power loading [N/kW]	N/A	N/A	94.0	156.2
Battery power loading [N/kW]	N/A	N/A	389.4	∞
Gas turbine power [MW]	4.13	4.12	4.79	4.81
Generator power [MW]	N/A	N/A	2.02	1.40
Electromotor power [MW]	N/A	N/A	2.52	1.33
Battery power [MW]	N/A	N/A	0.61	0
Average cruise lift-to-drag ratio [-]	17.86	18.45	18.41	18.50
Average cruise propulsive efficiency [-]	0.850	0.850	0.825	0.851
Cruise altitude [ft]	17,000	21,500	17,000	18,000
TV angle during take-off [deg]	N/A	N/A	0	10
TV angle during landing [deg]	N/A	N/A	30	55
Fuel energy [GJ]	70.2	69.2	84.6	70.6
Battery energy [GJ]	0	0	1.09	0
Degree-of-hybridization [-]	0	0	0.013	0
Payload-range energy efficiency [-]	2.11	2.15	1.76	2.13

This article has been cited by:

1. Bharath Govindarajan, Ananth Sridharan. Hybrid Powertrain Systems for Hybrid VTOL Aircraft . [Abstract] [PDF] [PDF Plus]
2. Reynard de Vries, Nando van Arnhem, Tomas Sinnige, Roelof Vos, Leo L.M. Veldhuis. 2021. Aerodynamic Interaction Between Propellers of a Distributed-Propulsion System in Forward Flight. *Aerospace Science and Technology* 107009. [Crossref]
3. Reynard de Vries, Nando van Arnhem, Francesco Avallone, Daniele Ragni, Roelof Vos, Georg Eitelberg, Leo L. M. Veldhuis. 2021. Experimental Investigation of Over-the-Wing Propeller–Boundary-Layer Interaction. *AIAA Journal* **59**:6, 2169-2182. [Abstract] [Full Text] [PDF] [PDF Plus] [Supplementary Material]
4. Sören Bölk, Reynard de Vries, Nando v. Arnhem, Leo L. Veldhuis. Numerical Investigation of Propeller–Flap Interaction in Inclined Over-the-Wing Distributed-Propulsion Systems . [Abstract] [PDF] [PDF Plus]
5. D. Felix Finger, Carsten Braun, Cees Bil. 2020. Comparative Assessment of Parallel-Hybrid-Electric Propulsion Systems for Four Different Aircraft. *Journal of Aircraft* **57**:5, 843-853. [Abstract] [Full Text] [PDF] [PDF Plus]
6. Alessandro Sgueglia, Peter Schmollgruber, Nathalie Bartoli, Emmanuel Benard, Joseph Morlier, John Jasa, Joaquim R. R. A. Martins, John T. Hwang, Justin S. Gray. 2020. Multidisciplinary Design Optimization Framework with Coupled Derivative Computation for Hybrid Aircraft. *Journal of Aircraft* **57**:4, 715-729. [Abstract] [Full Text] [PDF] [PDF Plus]
7. Marek ORKISZ, Michał KUŹNIAR. 2020. 3E – A new paradigm for the development of civil aviation. *Combustion Engines* **181**:2, 3-10. [Crossref]
8. D. Felix Finger, Carsten Braun, Cees Bil. 2020. Impact of Battery Performance on the Initial Sizing of Hybrid-Electric General Aviation Aircraft. *Journal of Aerospace Engineering* **33**:3, 04020007. [Crossref]
9. Hugo F. Bento, Reynard de Vries, Leo L. Veldhuis. Aerodynamic Performance and Interaction Effects of Circular and Square Ducted Propellers . [Abstract] [PDF] [PDF Plus]
10. Reynard de Vries, Maurice Hoogreef, Roelof Vos. Aero-Propulsive Efficiency Requirements for Turboelectric Transport Aircraft . [Abstract] [PDF] [PDF Plus]
11. Maurice Hoogreef, Reynard de Vries, Tomas Sinnige, Roelof Vos. Synthesis of Aero-Propulsive Interaction Studies Applied to Conceptual Hybrid-Electric Aircraft Design . [Abstract] [PDF] [PDF Plus]
12. D. Felix Finger, Carsten Braun, Cees Bil. Comparative Assessment of Parallel-Hybrid-Electric Propulsion Systems for Four Different Aircraft . [Abstract] [PDF] [PDF Plus]
13. Reynard de Vries, Nando van Arnhem, Francesco Avallone, Daniele Ragni, Roelof Vos, Georg Eitelberg, Leo L. Veldhuis. Aerodynamic Interaction Between an Over-the-Wing Propeller and the Wing Boundary-Layer in Adverse Pressure Gradients . [Citation] [PDF] [PDF Plus]
14. Maurice Hoogreef, Roelof Vos, Reynard de Vries, Leo L. Veldhuis. Conceptual Assessment of Hybrid Electric Aircraft with Distributed Propulsion and Boosted Turbofans . [Citation] [PDF] [PDF Plus]
15. Nando v. Arnhem, Roelof Vos, Leo L. Veldhuis. Aerodynamic Loads on an Aft-Mounted Propeller Induced by the Wing Wake . [Citation] [PDF] [PDF Plus]
16. Jacopo Zamboni, Roelof Vos, Mathias Emeneth, Alexander Schneegans. A Method for the Conceptual Design of Hybrid Electric Aircraft . [Citation] [PDF] [PDF Plus]